HIGH-Q MICROMECHANICAL RESONATORS AND FILTERS FOR ULTRA HIGH FREQUENCY APPLICATIONS

A THESIS

SUBMITTED TO THE DEPARTMENT OF ELECTRICAL AND

ELECTRONICS ENGINEERING

AND THE INSTITUTE OF ENGINEERING AND SCIENCES

OF BILKENT UNIVERSITY

IN PARTIAL FULFILLMENT OF THE REQUIREMENTS

FOR THE DEGREE OF

MASTER OF SCIENCE

By

Vahdettin Taş

August 2009

I certify that I have read this thesis and that in my opinion it is fully adequate, in scope and in quality, as a thesis for the degree of Master of Science.

Prof. Dr. Abdullah Atalar(Supervisor)

I certify that I have read this thesis and that in my opinion it is fully adequate, in scope and in quality, as a thesis for the degree of Master of Science.

Prof. Dr. Adnan Akay

I certify that I have read this thesis and that in my opinion it is fully adequate, in scope and in quality, as a thesis for the degree of Master of Science.

Prof. Dr. Ekmel Ozbay

Approved for the Institute of Engineering and Sciences:

Prof. Dr. Mehmet Baray
Director of Institute of Engineering and Sciences

ABSTRACT

HIGH-Q MICROMECHANICAL RESONATORS AND FILTERS FOR ULTRA HIGH FREQUENCY APPLICATIONS

Vahdettin Taş
M.S. in Electrical and Electronics Engineering
Supervisor: Prof. Dr. Abdullah Atalar
August 2009

Recent progresses in Radio Frequency Micro Electro Mechanical Sensors (RF MEMS) area have shown promising results to replace the off-chip High-Q macroscopic mechanical components that are widely used in the communication technology. Vibrating micromechanical silicon resonators have already shown quality factors (Q) over 10,000 at radio frequencies. Micromechanical filters and oscillators have been fabricated based on the high-Q micro-resonator blocks. Their fabrication processes are compatible with CMOS technology. Therefore, producing fully monolithic transceivers can be possible by fabricating the micromechanical components on the integrated circuits. In this work, we examine the general characteristics of micromechanical resonators and propose a novel low loss resonator type and a promising filter prototype. High frequency micromechanical components suffer from the anchor loss which limit the quality factor of these devices. We have developed a novel technique to reduce the anchor loss in extensional mode resonators. Fabrication processes of the suggested structures are relatively easy with respect to the current high-Q equivalents. The anchor loss

reduction technique does not introduce extra complexities to be implemented in the existing structures.

Keywords: Micromechanical Resonators, Micromechanical Filters, High-Q Resonator, Acoustic Transmission Lines, Anchor Loss

ÖZET

ÇOK YÜKSEK FREKANSLI UYGULAMALAR İÇİN YÜKSEK KALİTE FAKTÖRLÜ MİKROMEKANİK REZONATÖRLER VE FİLTRELER

Vahdettin Taş
Elektrik ve Elektronik Mühendisliği Bölümü Yüksek Lisans
Tez Yöneticisi: Prof. Dr. Abdullah Atalar
Ağustos 2009

Radyo Frekansı Mikro Elektro Mekanik Sensörler alanında yakın zamanda gerçekleşen gelişmeler, komünikasyon teknolojisinde geniş çapta kullanılan yüksek kalite faktorlü entegre edilemeyen makroskobik parçaların mikroskobik parçalarla yer değiştirmesi için umut verici sonuçlar göstermiştir. Radyo frekanslarında, 10,000'den fazla kalite faktörüne sahip titreşimli mikromekanik silikon rezonatörler üretilmiş durumdadır. Yüksek kalite faktörlü mikrorezonatörleri temel blok olarak kullanan mikromekanik filtreler ve osilatörler üretilmiş durumdadır. Bu elemanların üretim teknikleri CMOS teknolojisiyle uyumlu haldedir. Bu sebeple, mikromekanik elemanları entegre devrelerle beraber üreterek tek parça alıcı-vericiler üretmek mümkün olabilir. Bu çalışmada mikromekanik rezonatörlerin genel çalışma karakteristiği incelenmiş ve orijinal bir mikro rezonatör ve mikro filtre örneği tasarlanmıştır. Yüksek frekanslı mikromekanik rezonatörler, kalite faktörlerini belirleyen bağlantı kayıplarından dolayı performans sorunu yaşamaktadır. Çalışmamızda, uzama biçiminde titreşim gösteren rezonatörler için orijinal bir bağlantı kaybını azaltma tekniği

önerilmektedir. Önerilen yapıların üretim aşamaları mevcut eşleniklerininkine göre daha kolaydır. Bağlantı kaybını azaltma tekniği, mevcut yapılarda kullanımı için ekstra zorluklar doğurmamaktadır.

Anahtar Kelimeler: Mikromekanik Rezonatörler, Mikromekanik Filtreler, Yuksek Kalite Faktörlü Rezonatörler, Akustik İletim Hatları, Bağlantı Kayıpları

ACKNOWLEDGMENTS

I am sincerely grateful to Prof. Abdullah Atalar for his supervision, guidance, insights and support throughout the development of this work. His broad vision and profound experiences in engineering has been an invaluable source of inspiration for me. I would like to thank Dr. Ugur Toreyin for suggesting me to study with Prof. Atalar.

I am grateful to Prof. Hayrettin Koymen for his invaluable guidance and instructive advices throughout my study. The acoustic course taught by Prof. Koymen has constituted the fundamentals of this work. I would like to thank to the members of my thesis jury, Prof. Adnan Akay and Prof. Ekmel Ozbay for reviewing this dissertation and providing helpful feedback.

Many thanks to the members of our research group, Niyazi Senlik, Selim Olcum, Elif Aydogdu, Kagan Oguz, Burak Selvi, Deniz Aksoy and Ceyhun Kelleci for useful discussions, friendship and contributions to my work. I would like to especially acknowledge the contributions of Deniz Aksoy and Selim Olcum.

Thanks to Fazli, Omur, Altan, Ahmet and Can for their kind friendship.

Financial support of The Scientific and Technological Research Council of Turkey (TUBITAK) for the Graduate Study Scholarship Program is gratefully acknowledged.

Contents

1 INTRODUCTION **1**

1.2 Quality Factor 3

2 ANALYSIS OF A MICROMECHANICAL RESONATOR **7**

2.1 Small Signal Equivalent Circuit 9

2.2 Motional Resistance 12

2.3 Thermomechanical Noise of a Micromechanical Resonator 14

2.4 Spring Softening and Pull-in Effects of V_{DC} 15

2.5 Linearity, IIP_3 Point of Micromechanical Resonators 17

2.6 Coupled Resonators and Mode Splitting 19

3 REDUCING ANCHOR LOSS IN EXTENSIONAL MODE MICRORESONATORS **23**

3.1 Impedance, Area Mismatching 25

3.2 Mechanical quality factor of suspended resonators 31

3.2.1 Quarter-wavelength resonator 31

3.2.2 Half-wavelength resonator 32

3.2.3 Half-wavelength resonator supported with a quarter-wavelength bar 32

3.2.4 Half-wavelength resonator supported with three quarter-wavelength sections 33

3.2.5 Half-wavelength resonator supported with an odd number of quarter-wavelength sections 34

3.2.6 Odd-overtone resonances 34

3.3 Simulation Results 35

4 MICROMECHANICAL FILTER DESIGN 38

4.1 Introduction 38

4.2 Length Extensional Mode Resonator 38

4.2.1 Anchor Loss Calculation 39

4.2.2 Small Signal Electrical Equivalent Circuit 43

4.3 Filter Design 45

4.3.1 Coupling Beam Design 48

4.3.2 Two Port Representation of the Coupling Beams 50

4.3.3 Small Signal Equivalent Circuit of The Filter 52

4.3.4 Filter Design Example and Simulation Results 55

5 CONCLUSIONS 64

List of Figures

1.1 (a) A typical superheterodyne system.(b) The system implemented with micromachined structures [1]. 1

1.2 (a) The Resonant Gate Transistor with Q=90, $f_0 = 2.8kHz$ [2]. (b) Folded Beam Resonator with Q=80,000, $f_0 = 18kHz$ [3]. (c) Free-Free Beam Resonator Q=8,000, $f_0 = 92MHz$ [4]. (d) Length Extensional Rectangular Resonator Q=180,000, $f_0 = 12MHz$ [5]. (e) Elliptic Bulk-Mode Disk Resonator Q=45000, $f_0 = 150MHz$ [6] (f) Piezoelectric Contour Mode Ring Resonator Q=2900, $f_0 = 470MHz$ [7] (g) Material Mismatched Disk Resonator Q=11500, $f = 1.5GHz$ [8]. (h) Hollow Disk Ring Resonator Q=14600, $f_0 = 1.2GHz$ [9] 3

1.3 Elastic waves propagate through the substrate during the bending of the cantilever. 5

2.1 A typical resonator excited by electrostatic forces. 8

2.2 (a) Electrical Equivalent Circuit of the resonator in the figure 2.1. (b) Equivalent circuit seen from the input electrical side. 10

2.3 Coupled Pendulums illustrating mode splitting effect 20

2.4 a- Electrical Equivalent Circuit of the mass spring system in the figure 2.3. b- The same circuit redrawn to clarify the symmetric excitation. c- The odd mode. d- The even mode 21

2.5 Simulation result of the circuit in Fig. 2.4. The dashed line shows the result when coupling capacitance is tripled. 22

3.1 Lumped approximations of the distributed acoustic (a) and electrical (b) transmission lines. 24

3.2 The piezoelectric resonator suggested by Newel [10] to reduce the substrate loss. 27

3.3 The material mismatched disk resonator [10]. 28

3.4 Incident, reflected ($\mathcal{R}$) and transmitted ($\mathcal{T}$) pressure waves at a discontinuity in an acoustic bar of uniform thickness, T. 29

3.5 Calculated (solid line) and simulated (dots) reflection coefficients versus area ratio. 30

3.6 Electrical equivalent circuits of suspended resonators, (a) $\lambda/4$ resonator, (b) $\lambda/2$ resonator, (c) $\lambda/2$ resonator supported with a $\lambda/4$ bar. 33

3.7 (a) Electrical equivalent circuit of a half-wave resonator supported with three quarter-wave sections, (b) mode shape and stress distribution during elongation. 35

3.8 Axial symmetrical structure used to find Q_{anchor}. Line at the left shows the symmetry axis. 36

3.9 A comparison of finite element simulation results with the analytical formula: Q of silicon (E=150 GPa, ρ=2330 kg/m^3 and ν=0.3) resonators for varying λ^2/A_0 ratios. Q_0 of a quarter-wave resonator (lower curve), Q_1 of half-wave resonator with one $\lambda/4$ support with r=4 (middle curve), and Q_2 of half-wave resonator with three $\lambda/4$ supports with r=6.25 (upper curve) 37

4.1 Length Extensional Rectangular Resonator 39

4.2 Mode shape and stress distribution of a length extensional mode resonator. (a) Stress in the longitudinal,x, direction, (b) Stress in the transverse,y, direction. Green regions show the stress free regions. Stress is larger at the regions shown with darker colors. . 41

4.3 Equivalent electrical circuit of the resonator in the fig. 4.1. One half of the resonator is modeled since the resonator is perfectly symmetric. The gyrator has a ratio of k. 44

4.4 Length extensional mode resonator improved with area mismatched attachment beams. 46

4.5 Proposed filter type with excitation and detection electronics. . . 47

4.6 Mode shapes and stress distribution of the filter.(a) In symmetric mode, both resonators vibrate in phase. (b) In anti-symmetric mode the resonators vibrate with a phase difference of 180°. . . . 49

4.7 (a) Vibration shape of the coupling beam, the coupling beam is in flexural motion while the resonators vibrate in the elongation mode. (b) Equivalent two port representation of the coupling beams 51

4.8 The electrical equivalent circuit of the filter in the figure 4.5. . . . 53

4.9 (a) Transfer function of a single resonator. (b) Transfer function of a coupled two resonator system. (c) The coupled resonator system is terminated with resistors to obtain a flat filter characteristic. . . 54

4.10 (a) Response of the filter design with parameters given in the tables 4.1, 4.2. (b) Response of the same filter, terminated with 50Ω. 58

4.11 Flat filter response obtained with proper termination resistances 59

4.12 Response of a seventh order filter, compare with the response of the second order filter response shown in Fig. 4.10 (a). 60

4.13 The filter response for L_0=5μm, the efficiency of the low velocity coupling can be examined by comparing with the response shown in the fig. 4.10 (a). 61

4.14 (a) Feedthrough path through the wafer. (b) The feedthrough parasitics in the equivalent circuit. 62

4.15 The filter response with the feedthrough parasitics. Compare with the response in Fig. 4.10 (a). 62

4.16 Medium Scale Integrated Differential Disk Array Filter [11]. . . . 63

List of Tables

2.1 Electro-Mechanical Analog Components 10

3.1 Values of constants for different materials 31

4.1 Dimensional and Technological Parameters of the Sample Filter . 56

4.2 Component values of the equivalent circuit based on the values in Table 4.1 57

Dedicated to My Parents and Brothers

Chapter 1

INTRODUCTION

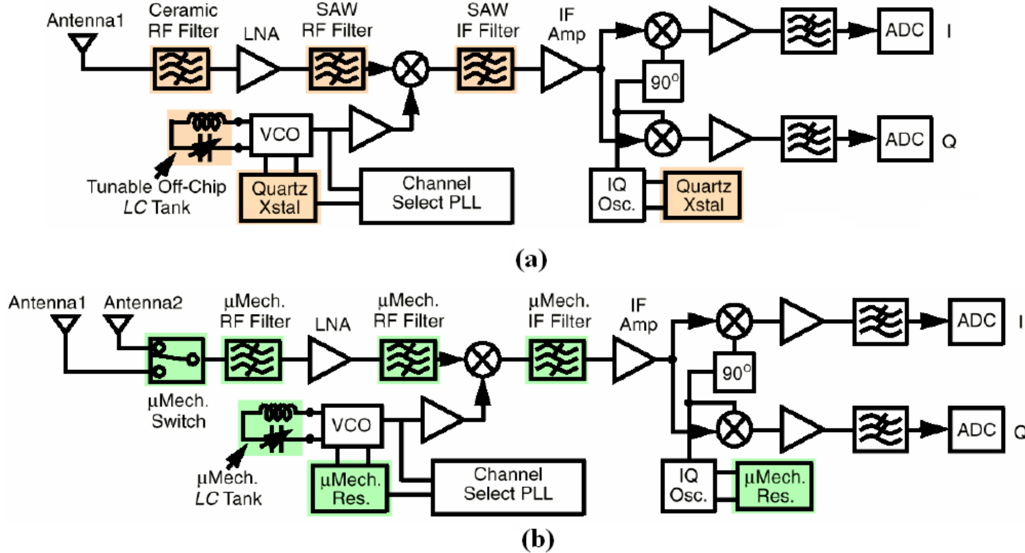

Figure 1.1: (a) A typical superheterodyne system.(b) The system implemented with micromachined structures [1].

With the advances in communication technology, the need to use the spectrum more efficiently has increased considerably which required devices with very high frequency selectivity. Great portion of the communication systems is based on superheterodyne principle. Fig. 1.1 (a) [1] illustrates a typical superheterodyne receiver system. The architecture has not been suitable to produce fully monolithic transceivers. The devices as LNA (Low Noise Amplifier), Mixers and

IF (Intermediate Frequency) amplifiers are fabricated with the CMOS technology. However, the filters and oscillators shaded with yellow color in the figure are not implementable with the CMOS technology. Main reason behind this is the need for low loss (high Q-factor) devices to achieve the high frequency selectivity and frequency stability (low phase noise). The need for high-Q components can not be met by the integrated electronic devices due to the lossy characteristics of electronic components at high frequencies. Low loss mechanical components as ceramic filters, surface acoustic wave (SAW) devices and crystal filters/oscillators are preferred instead. Besides being high-Q, these devices also show good performance in terms of temperature stability and aging [12].

Despite their performance, the off-chip components are disadvantageous in terms of cost and size as they are incompatible for on chip integration. They should be replaced with counterparts suitable for integration with IC's to benefit the advantages of single-chip devices as lower cost, lower size and less exposure to the parasitic effects. To avoid the macroscopic mechanical devices, several techniques have been proposed. Direct-conversion transceivers have been suggested [13] which offer to convert the RF signal to the baseband directly and avoid the RF-IF filters. This method has been used in some applications, however it is problematic concerning DC offsets and 1/f noise as the signal is amplified at the low frequency portion of the spectrum [14].

Another solution has arisen from the MEMS (Micro-Electro-Mechanical-Sensors) area. Recent progresses in RF MEMS are very promising to produce fully monolithic transceiver systems. Micromechanical filters and oscillators have been fabricated by integrated circuit compatible techniques [15, 16, 17, 18] which showed their potential to replace off-chip surface acoustic wave or crystal devices. Thermal stability and aging characteristic of these devices are also in competition with the macroscopic counterparts [19]. Fig. 1.1 (*b*) shows a possible superheterodyne system implemented with the vibrating micromechanical devices.

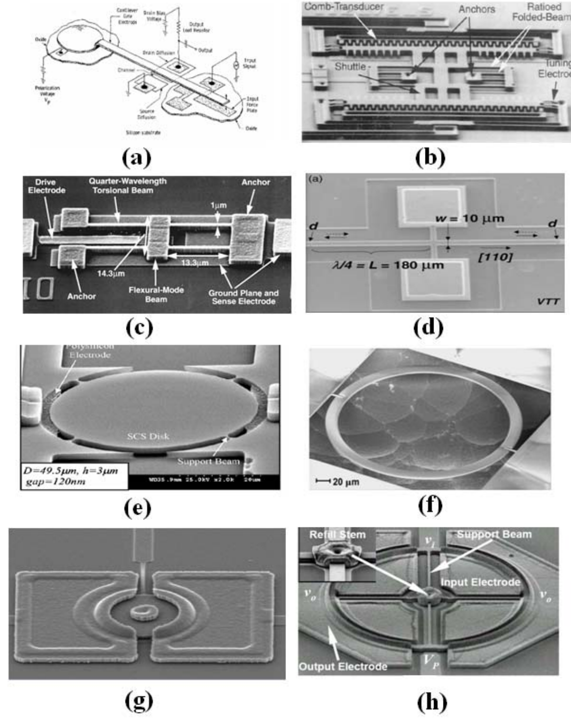

Figure 1.2: (a) The Resonant Gate Transistor with Q=90, $f_0 = 2.8kHz$ [2]. (b) Folded Beam Resonator with Q=80,000, $f_0 = 18kHz$ [3]. (c) Free-Free Beam Resonator Q=8,000, $f_0 = 92MHz$ [4]. (d) Length Extensional Rectangular Resonator Q=180,000, $f_0 = 12MHz$ [5]. (e) Elliptic Bulk-Mode Disk Resonator Q=45000, $f_0 = 150MHz$ [6] (f) Piezoelectric Contour Mode Ring Resonator Q=2900, $f_0 = 470MHz$ [7] (g) Material Mismatched Disk Resonator Q=11500, $f = 1.5GHz$ [8]. (h) Hollow Disk Ring Resonator Q=14600, $f_0 = 1.2GHz$ [9]

In terms of quality factor, micromachined resonators have shown superior performance at radio frequencies. Which showed their potential to select the channels at directly RF and simplify the transceiver electronics significantly [20, 9]. Fig. 1.2 illustrates the remarkable resonators in the development of micromechanical resonators.

1.2 Quality Factor

The main performance measure of the resonators is the quality factor, Q, which equals

$$Q = 2\pi \frac{\text{Stored Energy}}{\text{Energy Lost per Cycle}} \tag{1.1}$$

The definition implies that Q is the number of cycles, a resonator builds up energy. As Q increases the number of cycles of energy storage increases, hence the bandwidth of the frequency response decreases. This results another equivalent definition of the quality factor in terms of frequency parameters: $Q = w_0/BW$, where w_0 is the center frequency of the resonator and BW is the 3-dB bandwidth. Therefore Q is the main parameter for the frequency selectivity. A high quality factor also means low loss, hence less exposure to the thermomechanical noise which degrades the sensitivity.

In order to replace SAW and crystal components the micromachined resonators should be designed to have high quality factors. The energy dissipation mechanisms which determine the quality factor in micromachined structures are the air damping, the anchor loss, the thermoelastic dissipation, the surface loss and the internal (material) dissipation [21].

Bulk mode extensional resonators have reached very high quality factors [5]. Their stiffness, in the order of 10^6 N/m, enables these resonators store a high amount of energy. With this characteristic, in contrast to the flexural resonators, bulk extensional ones can achieve very high Q values with the same amount of air damping per cycle [16, 22] at high frequencies. As the surface to volume ratio of the bulk extensional mode resonators is low, surface losses do not pose a limitation on the quality factor. Another loss mechanism, thermoelastic dissipation is the result of an irreversible heat flow due to the stress gradients in micromechanical resonators. A recent work has shown that the thermoelastic dissipation in the bulk extensional resonators is also too low to limit Q [23]. Fabricating the micro-resonators from low loss materials such as silicon, material dissipation can be kept at low values. Silicon micromechanical resonators with

quality factors of 10,000 at GHz frequencies have been implemented [9], even at these high frequencies material losses do not limit Q value.

At high frequencies, the main loss mechanism which determines the quality factor in extensional mode resonators is the anchor loss [24]. Which is caused by the propagation of the elastic waves through the substrate. The wafers are infinitely large with respect to the resonators attached to them. Therefore, the energy coupled to the substrate is lost before reflecting from the boundaries of the wafer and returning back to the resonator. Fig. 1.3 illustrates a cantilever in the flexural mode. Bending of the cantilever causes stress waves propagating through the wafer that causes the anchor loss.

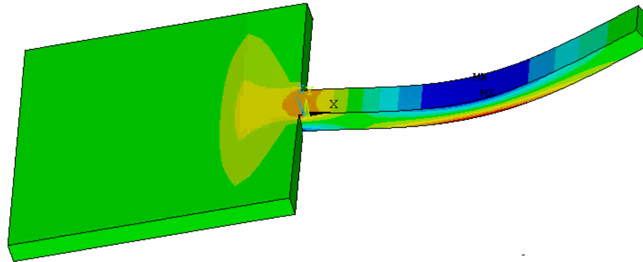

Figure 1.3: Elastic waves propagate through the substrate during the bending of the cantilever.

Several designs have been implemented to eliminate the anchor loss in micromachined structures. Resonators have been attached at their nodal points [16, 25] to reduce the energy coupled to the substrate. Impedance mismatching methods have been used in several designs. Newell suggested using Bragg reflectors composed of different material types [10]. Wang et al. have implemented material mismatched disk resonators [8]. Reflection property of the quarter wavelength beams have been used to reduce support loss in [9, 20]. In another work, thinner beams have been used to attach bulk micromachined resonators to the substrate [26]. Principles of these designs will be explained in the following chapters.

This thesis focuses on vibrating micromechanical resonators and filters with low anchor loss. Main contributions of this work are introducing a novel high-Q resonator and a high-Q coupled micromechanical filter and developing a technique to increase the quality factors of extensional mode micro-resonators.

The thesis will first explain the general characteristics of micromechanical resonators in Chapter-II. Chapter-III will introduce a new technique to enhance the quality factor of extensional resonators and analyze our micro-resonator design. Chapter IV will deal with the filter construction technique using high-Q micro resonators and will introduce our micromechanical filter design and simulation results.

Chapter 2

ANALYSIS OF A MICROMECHANICAL RESONATOR

Fig. 2.1 illustrates a typical micromechanical resonator. The resonator is a clamped-clamped beam anchored at both sides. The gap between the resonator and the fixed electrode forms a capacitor. The resonator is excited by applying an AC voltage to the fixed electrode and a DC bias to the resonator fabricated from a conductive material. The force between the electrodes equals the derivative of the stored energy in the capacitor with respect to displacement, x.

$$F = \frac{V^2}{2}\frac{\partial C(x,t)}{\partial x} \quad , \quad (V^2 = V_{DC}^2 + V_{AC}^2 - 2V_{DC}V_{AC}) \tag{2.1}$$

C is the capacitance between the plates;

$$C(x,t) = \frac{\epsilon_0 A}{d_0 + x} = \frac{C_0}{1 + x/d_0} \tag{2.2}$$

$$C_0 = \frac{\epsilon_0 A}{d_0} \tag{2.3}$$

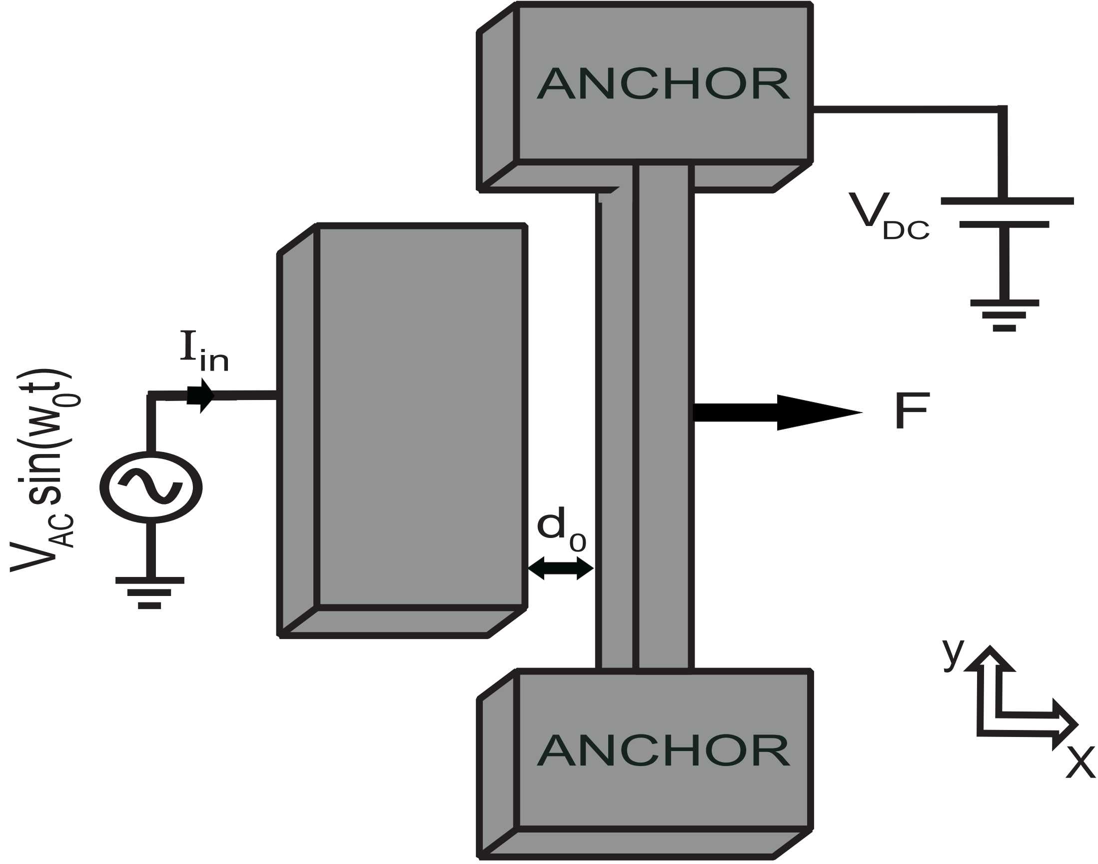

Figure 2.1: A typical resonator excited by electrostatic forces.

The equations should also include the y dependance as the displacement profile is not uniform for a clamped-clamped beam. However for simplicity of the analysis, uniform displacement is assumed, the y dependance can be inserted into the equations by analyzing the mode shape of the vibrating structure. C_0, d_0 are the static capacitance and the gap between the plates, ϵ_0 is the permittivity of the air, x is the vibration displacement and A is the cross sectional area of the resonator. The force has components at DC, excitation frequency and twice the excitation frequency. Choosing $V_{AC} \ll V_{DC}$ and applying frequencies around the resonance frequency of the resonator, the dominant component of the force is the one at the excitation frequency.

For small vibration amplitudes, $x \ll d_0$.

$$\frac{1}{1 + x/d_0} = 1 - \frac{x}{d_0} + \frac{x^2}{d_0^2} - \frac{x^3}{d_0^3} + \frac{x^4}{d_0^4} \quad - - - \tag{2.4}$$

To find the force, higher order terms of Eq. 2.4 can be neglected if small amplitude vibration is assured, first two terms are adequate. Combining the equations 2.4, 2.2 and 2.1, the force at the resonance frequency equals:

$$F = \frac{V_{DC} V_{AC} C_0}{d_0} \tag{2.5}$$

The total current passing through the voltage source equals the time derivative of the charge

$$I_{in} = \frac{\partial (C(x,t)V(t))}{\partial t} = (V_{DC} + V_{AC})\frac{\partial C(x,t)}{\partial t} + C(x,t)\frac{\partial V_{AC}}{\partial t} \tag{2.6}$$

I_{in} current is composed of two components. The first term (motional current) is due to the vibration of the resonator which will be related to the velocity of the resonator in the following part. The V_{AC} term can be neglected in the motional current expression for excitations with $V_{AC} \ll V_{DC}$. The second component of I_{in} is called the electrical current which is the result of the static capacitance between the plates.

2.1 Small Signal Equivalent Circuit

Electrical equivalent circuits can be constructed to represent the electromechanical systems. Fig. 2.2 shows the small signal electrical equivalent circuit of the resonator of Fig. 2.1. Small signal condition is stated to assure linearity. Force-Voltage equivalence has been used to constitute the electromechanical analogy. Table 2.1 lists the equivalent terms in the electrical and the mechanical domain. The clamped-clamped beam in the Fig. 2.1 has infinite number of modes. The

equivalent circuit models only the first mode of the resonator. Other modes of the resonator can be modelled by adding more RLC sets into the equivalent circuit [27]. However, representing the first mode is adequate for the applications explained in this thesis. Therefore, the beam can be modelled by lumped elements as a spring mass system and the relation between the force and the displacement equals

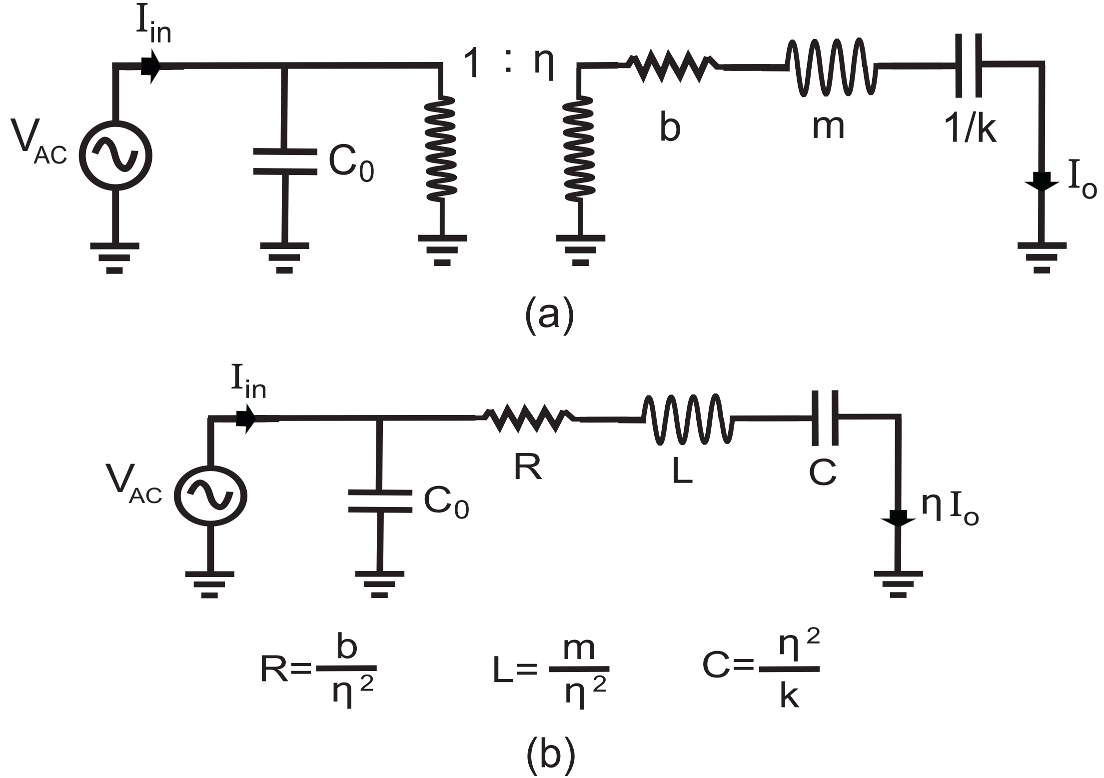

Figure 2.2: (a) Electrical Equivalent Circuit of the resonator in the figure 2.1. (b) Equivalent circuit seen from the input electrical side.

Table 2.1: Electro-Mechanical Analog Components

Mechanical Domain	*Electrical Domain*
Force	Voltage
Velocity	Current
Mass	Inductor
Compliance	Capacitor
Damping	Resistor

$$F = m\frac{\partial^2 x}{\partial t^2} + b\frac{\partial x}{\partial t} + kx \tag{2.7}$$

in phasor domain

$$X = \frac{F}{-mw^2 + jwb + k} \tag{2.8}$$

where m equals the equivalent mass , k is the spring constant, b is the loss term of the beam and w is the angular excitation frequency. k equals mw_0^2 where w_0 is the resonance frequency which can be found by Euler-Bernoulli equations. b equals mw_0/Q and Q is the quality factor of the beam which will be examined in detail in the following chapters. For a clamped-clamped beam, w_0 equals [4];

$$w_0 = 2.06\pi\frac{t}{L}\sqrt{\frac{E}{\rho}} \tag{2.9}$$

Where L and t are the length and thickness of the beam, E, ρ are the Young's modulus and density of the beam material.

Equivalent mass can be found by integrating the maximum kinetic energy along the beam and equating this energy to the kinetic energy of the mass-spring system.

$$\int_0^L \frac{1}{2}w^2 X(y)^2 dM = \frac{1}{2}mw^2 X_o \tag{2.10}$$

where L is the length of the beam, dM, $X(y)$ are the differential mass and displacement along the y direction and X_o is the displacement at the point where the lumped approximation is done. That is typically the center of the beam $(y = L/2)$.

In the equivalent circuit, C_0 represents the static capacitance, value of which is given in Eq. 2.2. C_0 models the electrical current in Eq. 2.6. I_0 is the motional

current which is the velocity of the beam. At resonance I_0 equals;

$$I_0 = \frac{FQw_0}{k} \tag{2.11}$$

Transformer with a $1 : \eta$ ratio interprets the transformation from the electrical domain to the mechanical domain across which voltage is converted to force and current is converted to velocity. Value of η can be extracted from Eq. 2.5;

$$F = \eta V_{AC} \tag{2.12}$$

So,

$$\eta = \frac{V_{DC}C_0}{d_0} \tag{2.13}$$

2.2 Motional Resistance

Micromechanical filters and oscillators have been designed based on the resonators as the one introduced in the previous part [28, 29, 16]. One of the main parameters determining the performance of these devices is the motional resistance R illustrated in the Fig. 2.2(b). With typical dimensions, R can be on the order of MΩ for extensional mode resonators [16]. In a typical filter application, two port devices are designed and output is taken from the third electrode. When the output electrode is terminated with the traditional 50Ω, the filter's performance degrades considerably. This will be explained in detail in the Chapter IV. Although the resonator itself is a high-Q block, due to the mismatch between the impedances, in-band transmission of the filters reduces drastically.

R value can be found from the circuit in the Fig. 2.2(b).

$$R = \frac{b}{\eta^2} = \frac{mw_0}{Q\eta^2} \tag{2.14}$$

$$R = \frac{b}{\eta^2} = \frac{m w_0 d_0^4}{Q V_{DC}^2 \epsilon_0^2 A^2} \tag{2.15}$$

There are several parameters to reduce the R value. The most influential one is the gap distance between the electrodes, d_0. With advance fabrication techniques, gap distance has been reduced to hundreds of Angstroms by several research groups [29, 24]. Increasing V_{DC} and capacitive area A are other trivial ways. In [20], micromechanical bars with thicknesses around $50\mu m$ has been implemented and impedances around 10kΩ has been achieved. V_{DC} values on the order of 100 volts has been used in some implementations. However, this is not a practical solution since these devices are designed to be integrated with IC which function with voltages around 5 volts. Filling the electrostatic gaps with materials that have high dielectric constant has also been tried [30]. The problem with this method is that the interaction of the resonator with the solid gap reduces the quality factor of the resonator due to anchor loss described in the first chapter.

Array techniques have also been improved to reduce the motional resistance [31]. Exciting n identical resonators and summing the outputs reduces the resistance value to R/n. However, this idea is based on the restriction that n resonators are perfectly identical. For example, for resonators with quality factors of 100,000, the resonance frequency mismatch between the resonators should be within 1/100,000 which is impossible considering the uncertainties in the fabrication processes. In the work of Demirci et al. [31], this problem has been partially solved by coupling the resonators mechanically with very stiff coupling beams.

2.3 Thermomechanical Noise of a Micromechanical Resonator

Finite quality factor of the micromechanical resonators results in thermomechanical noise. The amount of this noise can be calculated using the equipartition theorem [21]. The thermal energy of a mode of a micromechanical resonator equals $k_BT/2$ where k_B is the Boltzmann constant and T is the thermal equilibrium temperature in Kelvins. Expressing the energy of a micromechanical resonator with the mean squared strain energy

$$\frac{k_BT}{2} = \frac{k < x^2 >}{2} \tag{2.16}$$

$< x^2 >$ is the result of a noise force f_n with a white characteristic shaped by the transfer function of the mode which is given by the Eq. 2.8.

$$x^2(w) = \frac{f_n^2(w)}{(k - mw^2)^2 + (mw_0w/Q)^2} \tag{2.17}$$

So,

$$< x^2 >= \int_0^\infty \frac{f_n^2}{(k - mw^2)^2 + (mw_0w/Q)^2} \frac{dw}{2\pi} \tag{2.18}$$

By Eqs. 2.16 and 2.18 mean square noise power of f_n^2 in a band of B equals

$$f_n^2 = 4k_BTBmw_0/Q \tag{2.19}$$

The mean square Johnson noise of b in the equivalent circuit (Fig. 2.2(a)) in a band of B is

$$V_n^2 = 4k_BTBb = 4k_BTBmw_0/Q \tag{2.20}$$

Equivalence of Eqs. 2.19 and 2.20 show that noise characteristic of the mechanical resonators can be determined from their equivalent circuits.

2.4 Spring Softening and Pull-in Effects of V_{DC}

While calculating the electrostatic force (Eq. 2.5) between the vibrating resonator and the fixed electrode, only the first two terms of the Eq. 2.4 were used. However the third term should also been taken into account since it has the effect of changing the effective spring constant of the resonator. The force due to the x^2/d_0^2 term in Eq. 2.4 results in a force proportional to x that is equivalent to a spring force. By Eqs. 2.1, 2.2 and 2.4 electrical spring constant ,k_e, due to this term can be found [2] as

$$k_e = \frac{V_{DC}^2 \epsilon_0 A}{d_0^3} \tag{2.21}$$

Overall spring constant becomes

$$k_{eff} = k - k_e \tag{2.22}$$

Generally $k_e \ll k$. This modifies the resonance frequency of the resonator;

$$w_o = \sqrt{\frac{k - k_e}{m}} = \sqrt{\frac{k}{m}}\,(1 - \frac{k_e}{2k}) \tag{2.23}$$

Hence spring softening provides with a method to tune micromechanical resonators especially for ones with low k value. For extensional mode resonators, spring constant is very large, therefore the range of tuning is very limited.

There is a natural limit on the choice of V_{DC}. The former analysis is based on the assumption that the mechanical spring force of the resonator can counteract the electrostatic force. However, there exists a positive feedback between the electrostatic force and the DC bias. Increasing V_{DC} increases the the electrostatic force which decreases the gap between the plates and further increases the force. The positive feedback causes instability when the gap distance reduces below a certain fraction of the zero-bias gap distance d_0. Edge point of instability can be found by equating the spring constant to the derivative of the electrostatic force with respect to the capacitive gap. For a parallel plate capacitor

$$\frac{\partial}{\partial d}\frac{\epsilon_0 A V_{DC}^2}{d^2} = \frac{\partial k(d_0 - d)}{\partial d} \tag{2.24}$$

where d and d_0 are the instantaneous and the static gap distances. This equation shows that instability occurs at $d = 2d_0/3$. So, the pull-in voltage V_P equals;

$$V_P = \sqrt{\frac{8kd_0^3}{27\epsilon_0 A}} \tag{2.25}$$

The calculations have been done for parallel plate capacitors. When the displacement of the resonator is not uniform, which is the general case such as a clamped-clamped beam, the pull-in distance and voltage depends on the displacement profile of the resonator.

Several methods have been developed to increase the the travel distance of electrostatic resonators beyond the pull-in distances. Driving the resonators by charge instead of voltage has been proposed. In this case the force equation becomes; $F = q^2/(2\epsilon_0 A)$, (q being the amount of charge) and positive feedback is avoided [32]. For a parallel plate capacitor, this method ideally predicts a full gap travel range. However, for nonuniform displacement profiles positive feedback can not be avoided, pull-in occurs with a larger travel range with respect to the voltage drive case. In another work [33], connecting a capacitor in series with the resonator-fixed electrode capacitance has been proposed. The aim is to obtain a negative feed back control to counteract the positive feedback. As the resonator moves, the voltage on it decreases due to the voltage division between the fixed capacitance and the moving capacitance, hence a more stable operation can be achieved. This method suffers from parasitic capacitances explained in [33].

The pull-in effect does not pose a problem for micromechanical resonators discussed in this thesis because pull-in voltages are far beyond the linear operation limits of the resonators which is explained in the next section.

2.5 Linearity, IIP_3 Point of Micromechanical Resonators

This section will examine the nonlinearity in micromechanical resonators. Third order intermodulation products of micromechanical resonators have been examined in [34]. A similar analysis will be followed in this section. One of the main measures of the nonlinearity of a communication system is the third order intercept point, IIP_3. At this point, the magnitude of the third order signal equals the magnitude of the fundamental signal component.

Let a system be defined by the polynomial characteristic with input X and output Y

$$Y = a_0 + a_1 X + a_2 X^2 + a_3 X^3 + a_4 X^4 ... \tag{2.26}$$

For a resonator of center frequency w_0, If signals at frequencies w_0, w_1 and w_2 with the same magnitude A_0 are applied as the input, i.e $X = A_0 cos(w_0 t) + A_0 cos(w_1 t) + A_0 cos(w_2 t)$. The outputs that will determine the IIP_3 point will be at frequencies w_0 and $2w_1 - w_2$ with magnitudes

$$Y = a_1 A_0 cos(w_0 t) + \frac{3}{4} a_3 A_0^3 cos((2w_1 - w_2)t) \tag{2.27}$$

For w_1, w_2 interfering signals such that $2w_1 - w_2 = w_0$, a non-filterable signal will take place at the center frequency of the resonator. The magnitude of the undesired signal will equal to the fundamental component for the input amplitude of;

$$A_0 = \sqrt{\frac{4a_1}{3a_3}} \tag{2.28}$$

Vibration amplitude of micromechanical resonators are generally much smaller than the dimensions of the resonator, therefore the main cause of nonlinearity is not mechanical. The main cause is the nonlinearity of the capacitive transduction [34]. Examining Eqs. 2.1, 2.5 and 2.8, when $V_{AC} =$

$V_0cos(w_1t) + V_0cos(w_2t)$ the displacement will have components at w_1 and w_2. By Eq. 2.5 and 2.8 in phasor domain

$$X_{wi} = \frac{C_0V_{DC}V_0}{d_0(-mw_i^2 + jw_ib + k)} \tag{2.29}$$

Let

$$\frac{1}{-mw_i^2 + jw_ib + k} = H(w_i)e^{j\phi(w_i)} \tag{2.30}$$

where $H(w_i)$ and $\phi(w_i)$ are the magnitude and phase of the transfer function at w_i. So the vibration amplitude due to $V_{AC} = V_0cos(w_1t) + V_0cos(w_2t)$ becomes

$$x = \frac{C_0V_{DC}V_0}{d_0}[H(w_1)cos(w_1t + \phi(w_1)) + H(w_2)cos(w_2t + \phi(w_2))] \tag{2.31}$$

Combining Eqs. 2.1,2.4 and 2.31, the force equals

$$F = C_0\frac{(V_{DC} - V_0cos(w_1t) - V_0cos(w_2t))^2}{2}[\frac{-1}{d_0} + \frac{2x}{d_0^2} - \frac{3x^2}{d_0^3} + \frac{4x^3}{d_0^4}] \tag{2.32}$$

The forces at the third intermodulation frequency $(2w_1 - w_2)$ will emerge due to the terms containing $cos^2(w_1t)cos(w_2t)$ dependence. Then F at this frequency is

$$F = \frac{3V_0^3C_0^4V_{DC}^5}{2d_0^7}H(w_1)^2H(w_2)\ cos[(2w_1 - w_2)t + 2\phi(w_1) - \phi(w_2)] \tag{2.33}$$

$$+\frac{6V_0^3C_0^3V_{DC}^3}{d_0^5}H(w_1)H(w_2)cos[(2w_1 - w_2)t + \phi(w_1) - \phi(w_2)] \tag{2.34}$$

$$+\frac{V_0^3C_0^2V_{DC}}{2d_0^3}H(w_2)cos[(2w_1 - w_2)t - \phi(w_2)] \tag{2.35}$$

The fundamental component of the force equals

$$F = \frac{C_0V_{DC}V_0cos(w_0t)}{d_0} \tag{2.36}$$

Equating Eqs. 2.36 and 2.35 the IIP_3 voltage can be found. The equations are cumbersome, but they are helpful to understand the effect of different parameters on linearity. In the previous sections, it had been shown that to reduce the motional resistance d_0 should be decreased, V_{DC} and capacitive area should be increased. Examination of the above equations show that decreasing d_0 and

increasing V_{DC} degrades linearity considerably. Eq. 2.35 tells that increasing the capacitive area does not degrade the linearity (In the equations area terms in C_0 cancel with the transfer functions). Therefore the best way to reduce motional resistance without degrading the linearity is to increase the capacitive area. Another way is to make arrays of resonators [31].

2.6 Coupled Resonators and Mode Splitting

Previous sections has dealt with the single resonator types. This section will cover a brief discussion on coupled resonators. When identical type of resonators are connected together by means of specific coupling structures, the overall resonator has additional modes. This behavior is called *mode splitting*. The number of modes equals the number of resonators coupled together. This section will deal with a two resonator case. Fig. 2.3(a) shows two pendulums coupled with a spring of spring constant k_c. The overall resonator vibrates at two modes. Fig. 2.3(b) shows the so called *even mode* at which both pendulums vibrate in phase. The coupling spring effectively has no effect on the motion. In (c), the *odd mode* is illustrated. In this case the pendulums vibrate out of phase and the center of the coupling spring is motionless. The coupling spring constant seen by each pendulums becomes $2k_c$. There are a number of great lectures on coupled oscillators[1] that are rich of visual examples.

Fig. 2.4 is the electrical equivalent of the pendulum system in Fig. 2.3. Mode splitting phenomenon can be examined also in this circuit using even-odd mode analysis. Fig. 2.4(b) which is equivalent to (a) has been drawn to clarify the symmetry axis which is the composition of the excitation schemes in (c) and (d). (c) illustrates the odd-mode excitation at which currents on the resonators flow in the reverse direction. (d) shows the even mode scheme at which currents are in

[1]http://ocw.mit.edu/OcwWeb/Physics/8-03Fall-2004/VideoLectures/index.htm

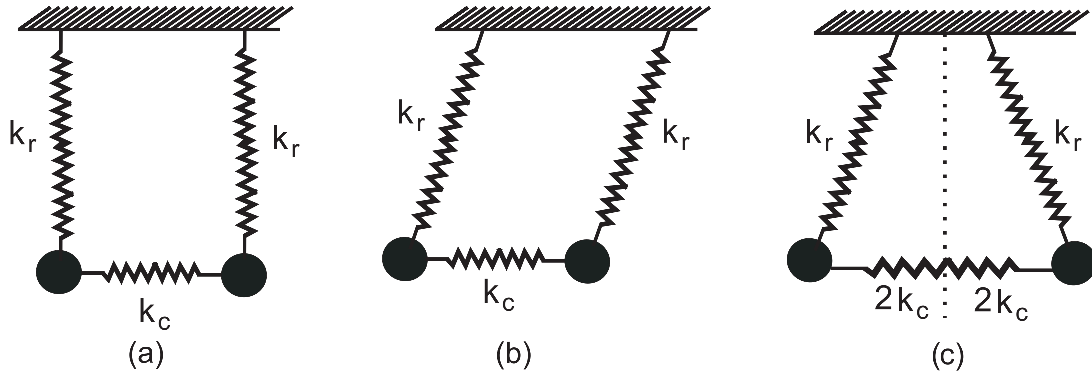

Figure 2.3: Coupled Pendulums illustrating mode splitting effect

the same direction. In the even mode, symmetry axis becomes a virtual ground hence the coupling capacitor (C_0) has no effect on the resonance frequency. In the odd mode, symmetry axis becomes open circuit, the coupling capacitor becomes in series with the resonator capacitance. The resonance frequencies are

$$w_{even} = \frac{1}{\sqrt{LC}} \tag{2.37}$$

$$w_{odd} = \frac{1}{\sqrt{L\frac{CC_0/2}{C+C_0/2}}} = \frac{\sqrt{1+2C/C_0}}{\sqrt{LC}} \tag{2.38}$$

For $2C \ll C_0$, which is the case for the coupled filters discussed in this thesis

$$w_{odd} \simeq \frac{1+C/C_0}{\sqrt{LC}} = (1+\frac{C}{C_0})w_{even} \tag{2.39}$$

Eq. 2.39 reveals that the spacing between the modes is proportional to $1/C_0$, which is k_c in the mechanical domain. The stiffer the coupling is, the modes are further from each other. The circuit in Fig. 2.4 (a) has been simulated for two cases. Fig. 2.5 shows the results. The only difference between the cases is that for the first one (dashed line) the coupling strength is one third of the second one. As the Eq. 2.37 expects, the even modes (first peaks in the figure) occur at the same frequency. The spacing between the odd mode and even mode is triple for the low capacitance case as revealed in Eq. 2.39.

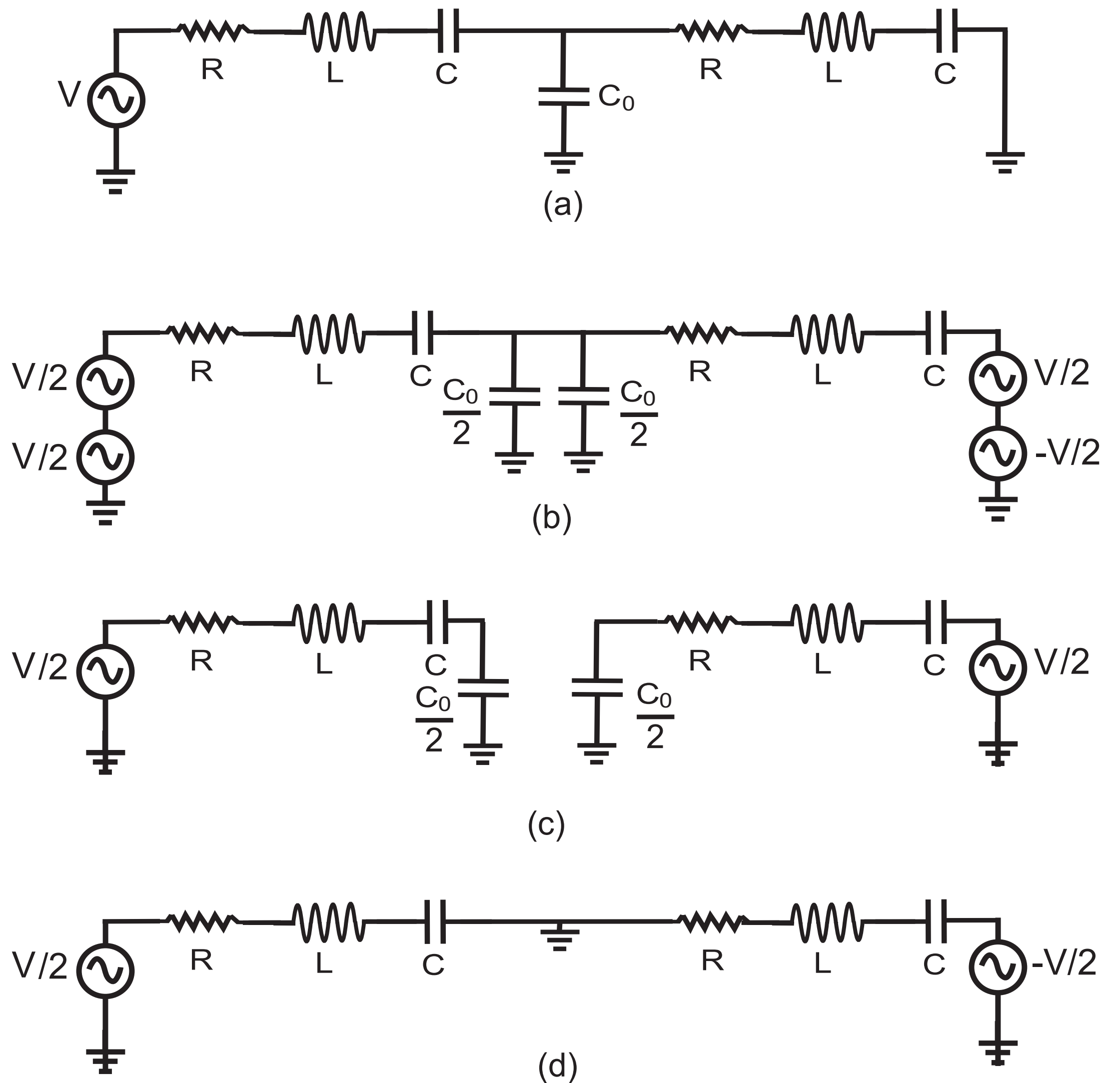

Figure 2.4: a- Electrical Equivalent Circuit of the mass spring system in the figure 2.3. b- The same circuit redrawn to clarify the symmetric excitation. c- The odd mode. d- The even mode

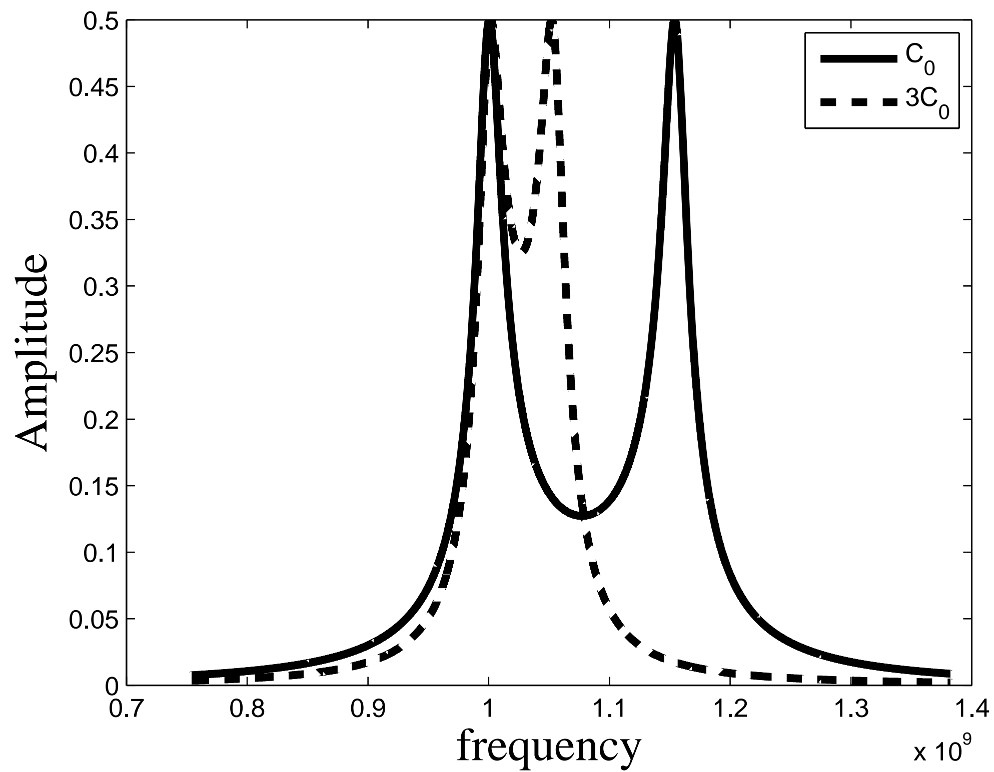

Figure 2.5: Simulation result of the circuit in Fig. 2.4. The dashed line shows the result when coupling capacitance is tripled.

Chapter 3

REDUCING ANCHOR LOSS IN EXTENSIONAL MODE MICRORESONATORS

Mechanical bars with length values much greater than the other dimensions show similar properties with the electrical transmission lines (TL), in a specific frequency range. This can provide with the usage of the well known techniques in Microwave Engineering, for the design of mechanical systems. Micromechanical transmission lines have been analyzed in [35]. This chapter will focus on the impedance and impedance mismatching concepts in acoustic transmission lines to reduce anchor losses in micromechanical resonators. The chapter starts by showing the analogy in both domains.

Wave equations in both electrical and mechanical TLs are in the same form. This can be illustrated with a simple lumped element approach. Fig. 3.1 illustrates the lumped element approximations of the acoustic (a) and electrical (b) transmission lines. Lumped elements of the electrical transmission lines are capacitors and inductors while masses and springs are the elements of the acoustic

transmission lines. Losses are neglected in the systems which could be modeled with the damping elements (resistors-dashpots). In the figure, M, k, L, C represent per unit length mass, spring constant, inductance and capacitance respectively. F, U, V, I represent the force, velocity, voltage and current. Δx is the differential distance.

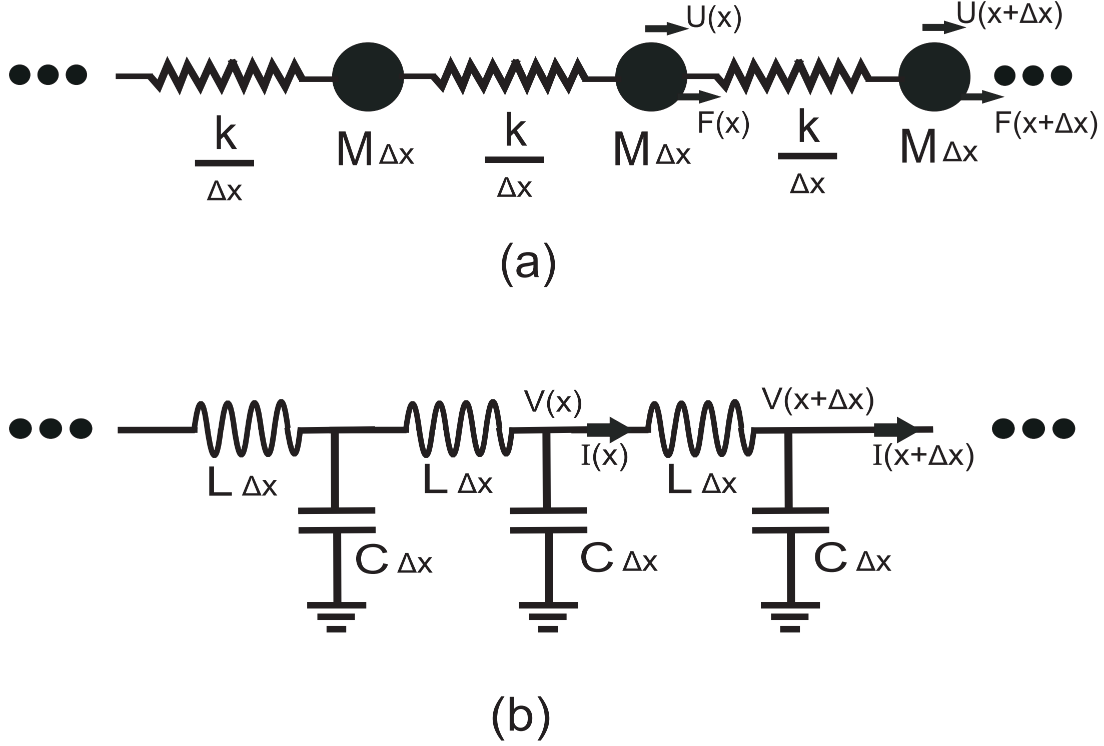

Figure 3.1: Lumped approximations of the distributed acoustic (a) and electrical (b) transmission lines.

For the mechanical case, Fig. 3.1(a), the governing equations in phasor domain for an excitation frequency of w are;

$$F(x + \Delta x) - F(x) = jwM\Delta x \; U(x + \Delta x) \tag{3.1}$$

$$U(x + \Delta x) - U(x) = \frac{jw\Delta x}{k} \; F(x) \tag{3.2}$$

For the electrical case, Fig. 3.1(b)

$$V(x) - V(x + \Delta x) = jwL\Delta x \; I(x) \tag{3.3}$$

$$I(x) - I(x + \Delta x) = jwC\Delta x \; V(x + \Delta x) \tag{3.4}$$

Eqs. 3.1 and 3.2 result in the wave equation

$$\frac{\partial^2 F(x)}{\partial x^2} + w^2 \frac{M}{k} F(x) = 0 \quad (3.5)$$

Eqs. 3.3 and 3.4 result in

$$\frac{\partial^2 V(x)}{\partial x^2} + w^2 LCV(x) = 0 \quad (3.6)$$

For an acoustic bar with uniform cross section, per unit length mass and spring constant for extensional excitations are

$$M = \rho A_0, \quad k = EA_0 \quad (3.7)$$

where A_0 is the cross sectional area, E and ρ are the Young's modulus and the density of the material. Eqs. 3.5 and 3.6 reveal that wave velocities for the mechanical and electrical cases are $\sqrt{k/m}$ ($= \sqrt{E/\rho}$) and $1/\sqrt{LC}$. Solving the wave equations for F and U, it is observed that the characteristic impedance, the amplitude ratio of the force and velocity waves propagating in the same direction, equals

$$Z_0 = \sqrt{kM} = A_0\sqrt{E\rho} = A_0 \frac{E}{c} \quad (3.8)$$

where c is the phase velocity. Z_0 has the unit of kg/sec. This is the analog of the characteristic impedance in the electrical domain which equals $\sqrt{L/C}$ [36].

3.1 Impedance, Area Mismatching

The above results are valid under specific conditions. Basically the analysis are consistent if a non-dispersive acoustic wave propagation is assured. In a thin rod, there may be a number of modes present depending on the frequency of excitation. The zeroth order longitudinal mode propagation is non-dispersive [37]. Higher and dispersive modes are excited above a certain frequency. Below this frequency all dispersive modes are evanescent. If the length of the rod, L is much

greater than its width, W, and its thickness, T ($T < W$), the closest higher order plate mode resonance occurs at $f_1 = f_o\sqrt{(1 + (L/W)^2)}$ [37] where f_o is the frequency at which L equals $\lambda/2$. If L/W is sufficiently large, f_1 is far away. For the zeroth order non-dispersive mode Eq. 3.8 is valid.

Impedance concept in acoustic rods gave us the idea to reduce anchor losses by increasing the impedance mismatch between a resonator and its substrate [38]. Impedance mismatching methods have been used in several designs. Newell suggested using Bragg reflectors composed of different material types [10]. Fig. 3.2 illustrates the proposed structure. Different material types with thicknesses of $\lambda/4$ are deposited on the substrate with alternating high and low impedances. Isolation from the substrate is determined by the number of layers and impedance mismatch between the layers. Solidly mounted resonators (SMR) have been fabricated based on this idea [39]. There are several problems with the SMRs. Their fabrication process is demanding, fabrication compatible materials with very different $\sqrt{E\rho}$ values are required. As the isolation is determined by the thickness of the layers, producing devices with varying frequencies in the same batch is too difficult since different thicknesses is required to achieve the $\lambda/4$ constraint for each frequency.

In another work, Wang et al. have implemented material mismatched disk resonators [8] shown in Fig. 3.3. Main body of the disk resonator is polydiamond whereas the stem at the center of the disk is made of polysilicon. Impedance mismatch between the polysilicon and the diamond reduced anchor loss considerably and a Q value of 11,555 was obtained at 1.5 GHz. Reflection property of the quarter wavelength beams have been used to reduce support loss in [9] and [4], however the mechanism behind reflection has not been explained explicitly.

In our design we use quarter-wavelength long strips with alternating low and high impedances to transform the impedance of the substrate to a very small value. Hence, the anchor of the resonator is connected to a very low

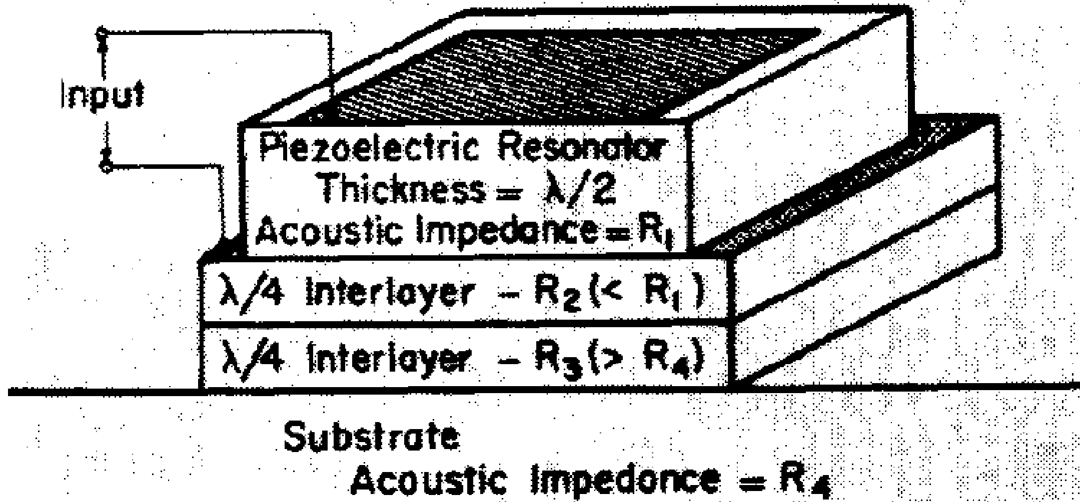

Figure 3.2: The piezoelectric resonator suggested by Newel [10] to reduce the substrate loss.

impedance and very little energy coupling occurs. Since the impedance of a strip is proportional to the width of the strip, we use alternating width strips with the same thickness to decouple the resonator from the substrate. The idea is similar to the acoustic Bragg reflector [10], however no other material type is required and the fabrication process is much simpler. More importantly, the resonance frequency of the resonators we propose are determined by lateral dimensions, hence multi-frequency applications can be implemented on the same chip . In what follows, a reflection mechanism in mechanical bars will be explained, based on this mechanism a novel resonator type with low anchor loss will be introduced.

Fig. 3.4 illustrates an infinitely long thin rod connected to another rod of the same thickness but of a smaller width. $A_1 = W_1T$ and $A_2 = W_2T$ represent the respective cross sectional areas of the rods. When a pressure plane wave is incident from the first strip to the second strip, the wave reflects with a reflection coefficient of R and transmitted to the second region with a transmission coefficient of T.

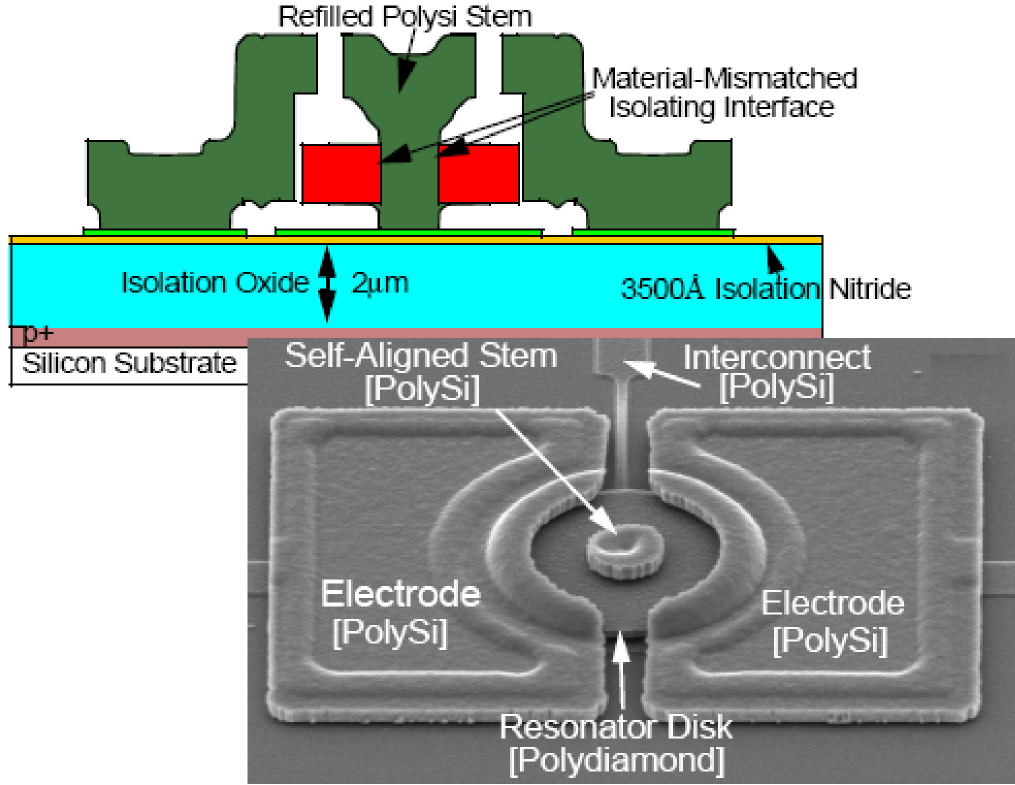

Figure 3.3: The material mismatched disk resonator [10].

A reflection occurs because both the force and the particle velocity should be preserved at the boundary [37]. We can write the boundary conditions as

$$f_1^+ + f_1^- = f_2^+ \quad v_1^+ - v_1^- = v_2^+ \tag{3.9}$$

where f and v stand for force and particle velocity, the superscripts $+$ and $-$ represent the direction of propagation, and the subscript refers to the first or second strip. For the zeroth order waves propagating in semi-infinite rods, the ratio of the force to the particle velocity can be found from the equation 3.8,

$$f_1^+/(A_1 v_1^+) = f_1^-/(A_1 v_1^-) = f_2^+/(A_2 v_2^+) = \sqrt{E\rho} \tag{3.10}$$

Solving Eqs. 3.9 and 3.10, the reflection and transmission coefficients of the force, R and T, can be found:

$$\mathcal{R} = \frac{f_1^-}{f_1^+} = \frac{(A_2 - A_1)}{(A_1 + A_2)} \quad \mathcal{T} = \frac{f_2^+}{f_1^+} = \frac{2A_2}{(A_1 + A_2)} \tag{3.11}$$

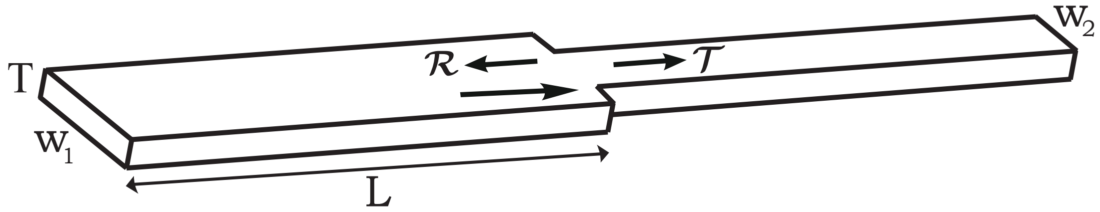

Figure 3.4: Incident, reflected ($\mathcal{R}$) and transmitted ($\mathcal{T}$) pressure waves at a discontinuity in an acoustic bar of uniform thickness, T.

i.e

$$\mathcal{R} = \frac{Z_2 - Z_1}{Z_1 + Z_2} \quad \mathcal{T} = \frac{2Z_2}{Z_1 + Z_2} \tag{3.12}$$

It is clear from this equation that $\mathcal{R}$ must be made as far as possible from zero to minimize the transmitted power. A transient analysis was done to examine the validity of Eq. 3.12 using a finite element package [1]. Fig. 3.5 shows the finite element simulation results along with the reflection coefficient values from Eq. 3.12 for various Z_2/Z_1 values. We can see that the first order approximation of Eq. 3.8 is valid in a wide range $0.02 < Z_2/Z_1 < 50$.

The rods are typically clamped to a substrate. If the substrate is sufficiently large, we can assume it to be infinitely large. Under this condition any energy coupled to the substrate can be considered to be lost. Hence, the substrate connection can be modeled as a resistance in the analogous electrical circuit. To complete the picture we need to express the value of this resistance in the mechanical domain. The substrate is modeled with a pure resistance because the waves entering to the substrate can not return back to the the resonator therefore there is no reactive power.

Suppose that the attachment point vibrates in response to uniform axial stress of σ_x at the clamped end. The corresponding force at the attachment is $\sigma_x A$. To calculate the displacement of the attachment, Hao et al. [40, 41] model the support as an infinite elastic medium. For a circular cross-section of area A, the

[1] www.ansys.com

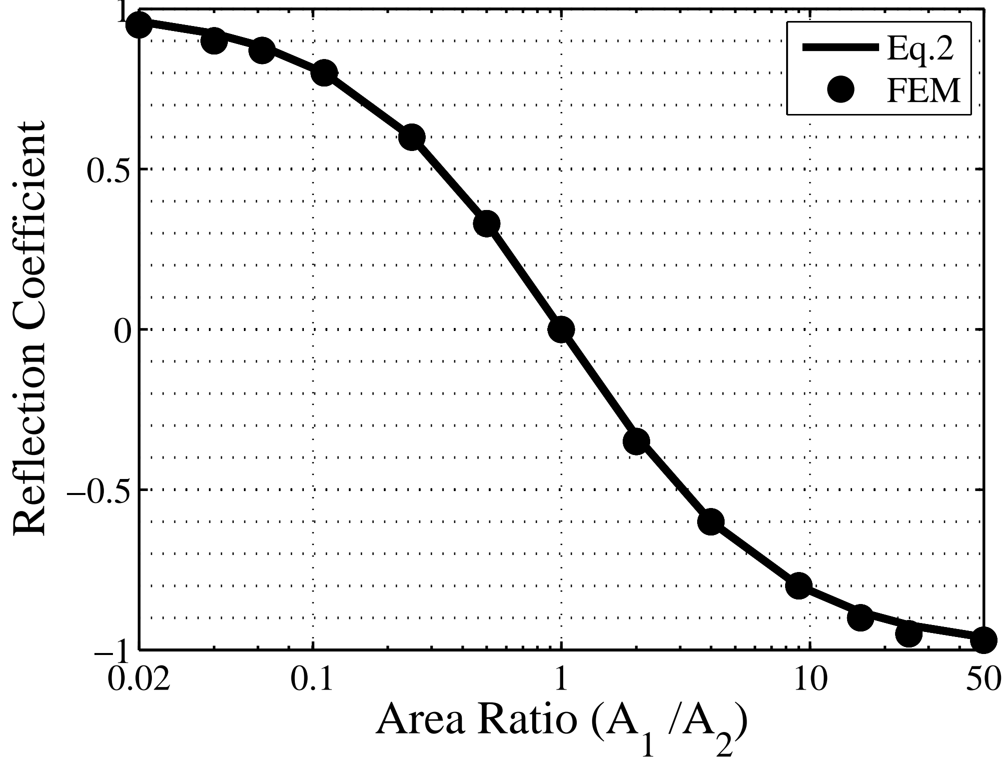

Figure 3.5: Calculated (solid line) and simulated (dots) reflection coefficients versus area ratio.

displacement of the attachment point is given by [40]

$$u_x = \frac{\sigma_x A \omega \gamma F(\gamma)}{2\pi\rho c_t^3} \tag{3.13}$$

with

$$c_t = \sqrt{\frac{E}{2\rho(1+\nu)}} \tag{3.14}$$

$$\gamma = \sqrt{\frac{2(1-\nu)}{1-2\nu}} \tag{3.15}$$

where ν is the Poisson ratio of the rod material and w isthe angular excitation frequency. $F(\gamma)$ is given by the imaginary part of an integral [40]:

$$F(\gamma) = Im \int_0^\infty \frac{\zeta\sqrt{\zeta^2-1}}{(\gamma^2-2\zeta^2)^2 - 4\zeta^2\sqrt{\zeta^2-\gamma^2}\sqrt{\zeta^2-1}}\, d\zeta \tag{3.16}$$

At this point we can define the equivalent resistance, R, representing the energy lost into the substrate. Its value can be found by dividing the force, $\sigma_x A$, by the

particle velocity, ωu_x:

$$R = \frac{2\pi c_t^3 \rho}{\gamma F(\gamma)} \frac{1}{\omega^2} = \frac{4}{\pi} \rho K c \lambda^2 \tag{3.17}$$

where

$$K = \frac{1}{16\sqrt{2}\gamma F(\gamma)(1+\nu)^{\frac{3}{2}}} \tag{3.18}$$

We check that the unit of R is kg/sec and it is consistent with the unit of Z. It is clear that R can be made large by choosing a high stiffness, low density material. We note that the quantities Z/A and R/λ^2 are dependent only on the material constants. Values of K, Z/A and R/λ^2 for a number of materials are listed in Table 3.1.

Table 3.1: Values of constants for different materials

Material	K	Z/A (kg/m^2/sec)	R/λ^2 (kg/m^2/sec)
Silicon Oxide	0.112	$1.24 \cdot 10^7$	$1.77 \cdot 10^6$
Silicon	0.101	$1.86 \cdot 10^7$	$2.41 \cdot 10^6$
Polysilicon	0.107	$1.92 \cdot 10^7$	$2.62 \cdot 10^6$
Silicon Nitride	0.106	$2.78 \cdot 10^7$	$3.75 \cdot 10^6$
Polydiamond	0.118	$6.20 \cdot 10^7$	$9.33 \cdot 10^6$

3.2 Mechanical quality factor of suspended resonators

3.2.1 Quarter-wavelength resonator

First, let us consider a resonator of quarter-wavelength long, $L = c/(4f) = \lambda/4$. The analogous electrical circuit is shown in Fig. 3.6(a). The mechanical quality factor, Q_0, of this resonator due to anchor loss can be found easily from the electrical equivalent to be

$$Q_0 = \frac{\pi}{4} \frac{R}{Z_0} \tag{3.19}$$

Using Eqs. 3.8 and 3.17 we find

$$Q_0 = K \frac{\lambda^2}{A_0} \tag{3.20}$$

It is clear that a high value of λ^2/A will result in a better quality factor. The resonator should have as small cross section as possible.

3.2.2 Half-wavelength resonator

In this case, $L = c/(2f) = \lambda/2$. The quality factor of the resonator (in Fig. 3.6(b)) from the electrical circuit is

$$Q = \frac{\pi}{2}\frac{Z_1}{R} \tag{3.21}$$

From Eqs. 3.8 and 3.17 we find

$$Q = \frac{\pi^2}{8K}\frac{A_1}{\lambda^2} \tag{3.22}$$

In this case, A_1/λ^2 must be large to have a high quality factor resonator. However, this requirement contradicts with the requirement that the length of the resonator should be much longer than its width to guarantee single mode operation. We conclude that a half-wavelength rod connected to a substrate directly does not result in a high Q resonator.

3.2.3 Half-wavelength resonator supported with a quarter-wavelength bar

We now combine the cases above to get a better resonator as depicted in Fig. 3.6(c) The electrical Q of this pair of resonators is given by

$$Q_1 = \frac{\pi}{4}\frac{R}{Z_0}\left(1 + \frac{2Z_1}{Z_0}\right) \tag{3.23}$$

Using Eqs. 3.8 and 3.17 we find

$$Q_1 = K\frac{\lambda^2}{A_0}(1 + 2r) \tag{3.24}$$

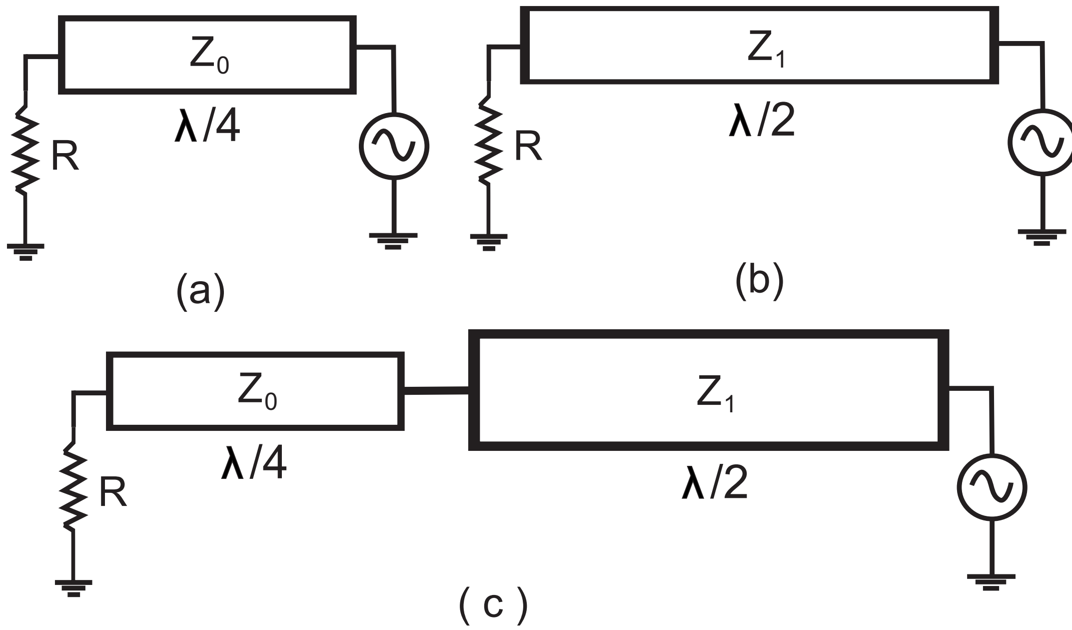

Figure 3.6: Electrical equivalent circuits of suspended resonators, (a) $\lambda/4$ resonator, (b) $\lambda/2$ resonator, (c) $\lambda/2$ resonator supported with a $\lambda/4$ bar.

with $r = A_1/A_0$. Clearly, the quality factor improves with λ^2/A_0 as well as by the factor $(1 + 2r)$. Making the area ratio r as large as possible will result in a high Q resonator.

3.2.4 Half-wavelength resonator supported with three quarter-wavelength sections

We can add two more quarter-wavelength sections to improve the quality factor even more as shown in Fig. 3.7(a). From the electrical circuit of this two pairs of resonators we find

$$Q_2 = \frac{\pi}{4}\frac{R}{Z_0}\left(1 + \frac{Z_1}{Z_0} + (\frac{Z_2}{Z_0} + \frac{2Z_3}{Z_0})(\frac{Z_1}{Z_2})^2\right) \tag{3.25}$$

Using Eqs. 3.8 and 3.17 we find

$$Q_2 = K\frac{\lambda^2}{A_0}\left(1 + \frac{A_1}{A_0} + (\frac{A_2}{A_0} + \frac{2A_3}{A_0})(\frac{A_1}{A_2})^2\right) \tag{3.26}$$

This equation shows that the area ratio between neighboring elements must be large to generate a high quality system. For the special case of $r = A_1/A_0 = A_3/A_2$ with $A_0 = A_2$, we find

$$Q_2 = K\frac{\lambda^2}{A_0}(1 + r + r^2 + 2r^3) \quad (3.27)$$

With a modest area ratio of r=5, the improvement in the quality factor is 281. Fig. 3.7(b) illustrates the mode shape and stress distribution of a resonator type working on this principle. Half-wavelength resonator is connected to the substrate through three quarter-wavelength sections. Harmonic analysis was done in the FEM simulator to observe the amount of stress at the clamped region. The stress at the anchor point is minimized by successful operation of the quarter-wavelength sections.

3.2.5 Half-wavelength resonator supported with an odd number of quarter-wavelength sections

We can generalize the formula of Eq. 3.27 to n pairs of resonators as follows:

$$Q_n = K\frac{\lambda^2}{A_0}(1 + r + r^2 + ... + r^{2n-2} + 2r^{2n-1}) \quad (3.28)$$

3.2.6 Odd-overtone resonances

The structures above resonate also at an odd multiple of the fundamental frequency. The corresponding quality factor at those frequencies can be determined easily from the electrical equivalent circuit. If the overtone resonance is at $(2m + 1)$ multiple, the quality factors of electrical equivalent circuits as given by Eqs. 3.19, 3.23 and 3.25 predict a quality factor improvement of $(2m + 1)$. However, the anchor loss represented by R is proportional to λ^2, and hence R decreases by the factor $(2m + 1)^2$ at these odd-overtones. We conclude that in

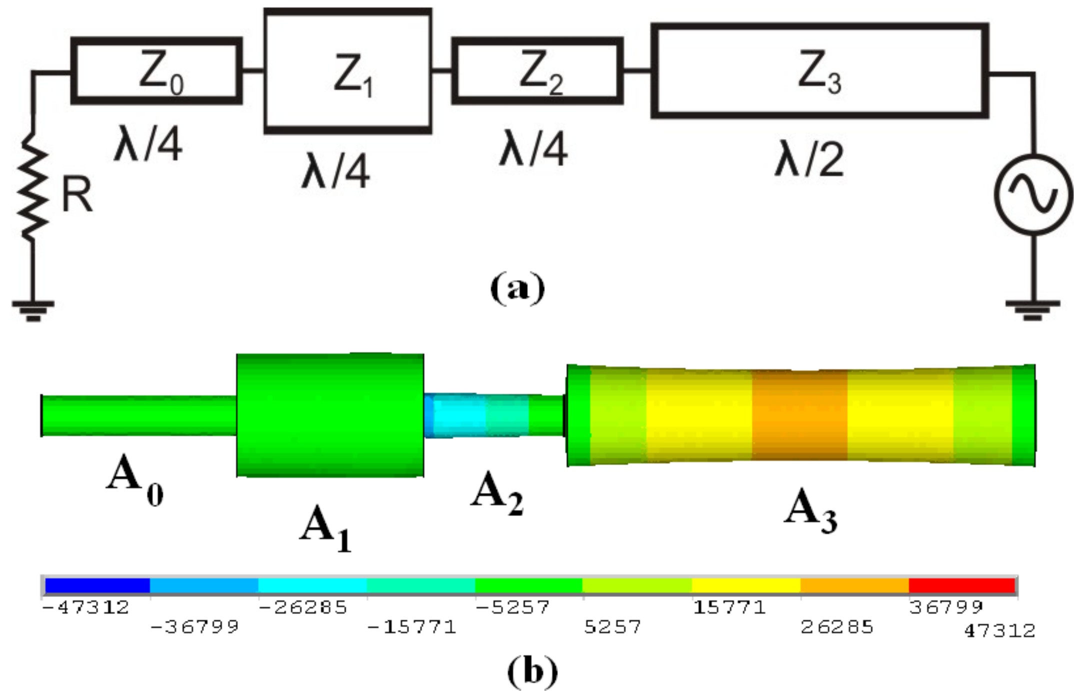

Figure 3.7: (a) Electrical equivalent circuit of a half-wave resonator supported with three quarter-wave sections, (b) mode shape and stress distribution during elongation.

all the structures above the quality factor at the $(2m+1)$th resonance is reduced by a factor of $1/(2m+1)$. So using overtone resonances is not advantageous. For example, the resonator of Fig. 3.6(c) ($3\lambda/4$ long) is better than a uniform three-quarter-wavelength (third-overtone) resonator.

3.3 Simulation Results

We have verified the validity of Eqs. 3.20, 3.24 and 3.27 by a finite element simulator. We used COMSOL[2] since it can handle a propagation into a semi infinite medium pretty well. Perfectly matched layers (PML) which are constructed by complex coordinate transformation have been implemented to find anchor loss [42]. In the FEM package, PML domains are available for several analysis types.

[2]www.comsol.com

We performed frequency response analysis to extract the quality factor. We worked with resonators with circular cross sections rather than rectangular to get axially symmetric structures for a better accuracy. Fig. 3.8 illustrates the model used in the simulation. Spherical substrate and PML domains have been used.

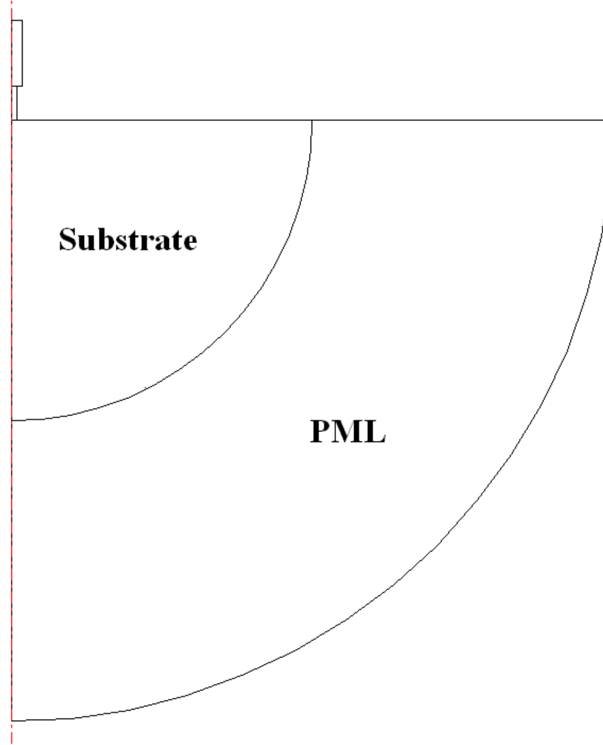

Figure 3.8: Axial symmetrical structure used to find Q_{anchor}. Line at the left shows the symmetry axis.

Fig. 3.9 is a comparison of Q values due to anchor loss, as obtained from the analytical expressions and the finite element simulation results. The quality factor of a silicon quarter-wave resonator at 250 MHz is plotted in the lower curve. For the half-wavelength resonator supported by a quarter-wavelength bar we chose r=4. Eq. 3.24 is plotted along with finite element simulation results in the middle of Fig. 3.9. In the same figure, a half-wavelength resonator with three quarter-wave support rods is also shown. We chose $A_0 = A_2$, $A_1/A_0 = 6.25$ and $A_1 = A_3$ (r=6.25). Differences between the curves and FEM results can be

attributed to the errors in simulations and deviations from the transmission line approximations as λ^2/A_0 ratio decreases.

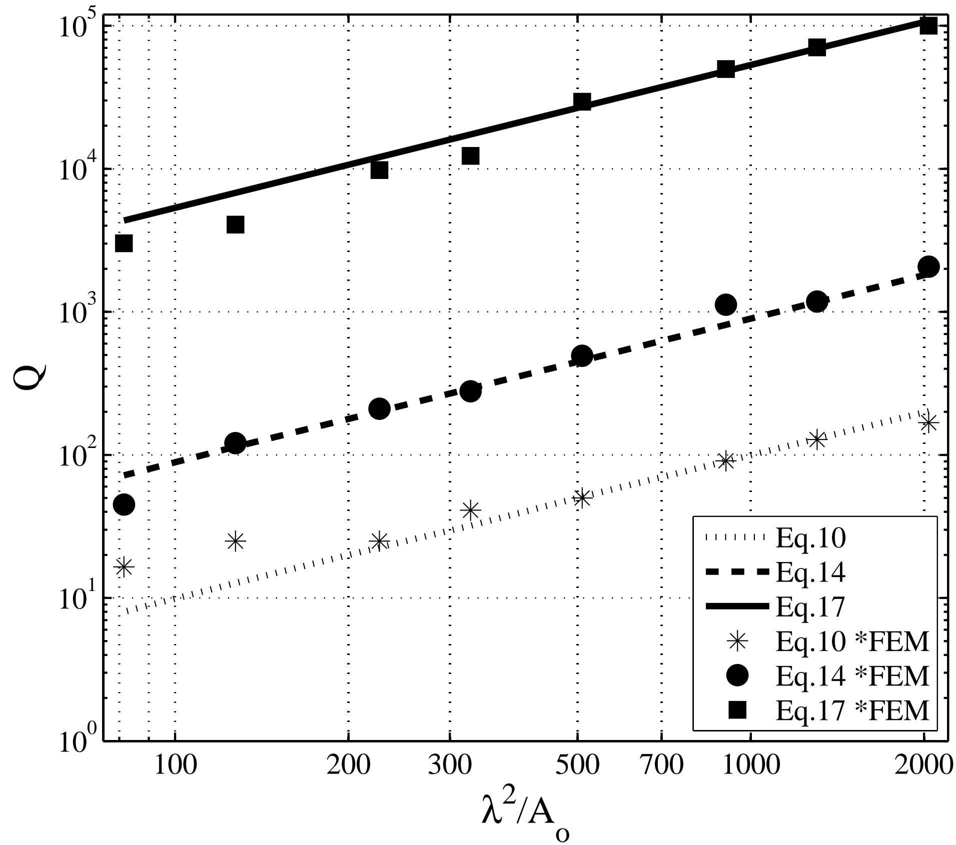

Figure 3.9: A comparison of finite element simulation results with the analytical formula: Q of silicon (E=150 GPa, ρ=2330 kg/m^3 and ν=0.3) resonators for varying λ^2/A_0 ratios. Q_0 of a quarter-wave resonator (lower curve), Q_1 of half-wave resonator with one $\lambda/4$ support with r=4 (middle curve), and Q_2 of half-wave resonator with three $\lambda/4$ supports with r=6.25 (upper curve)

Chapter 4

MICROMECHANICAL FILTER DESIGN

4.1 Introduction

In this chapter, length extensional mode rectangular resonators will be analyzed in detail. This resonator type has been fabricated and used as the high-Q block in the oscillator design of Matilla et.al [5] which has shown an impressive quality factor of 180,000 at 12 MHz (in vacuum). This structure is analyzed because it will constitute the main block of the micromechanical filters proposed in this thesis. In the following, anchor loss calculation of the rectangular extensional mode resonators will be done and an equivalent circuit will be introduced.

4.2 Length Extensional Mode Resonator

Fig. 4.1 shows the shape and the dimensions of the resonator introduced in [5]. The horizontal block with length $2L$ is the main resonating body and the vertical blocks are used to attach the resonator to the substrate. With symmetric

excitation at both arms of the resonator, symmetry axis remains stationary and this property reduces the anchor loss considerably.

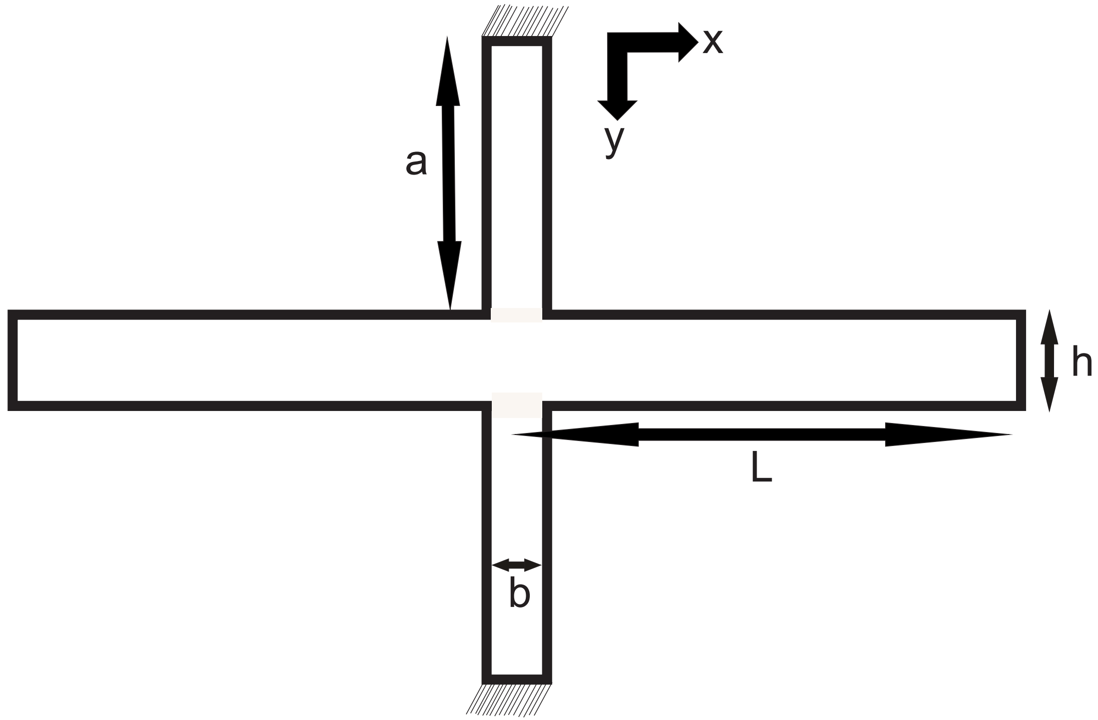

Figure 4.1: Length Extensional Rectangular Resonator

The resonator has been simulated in ANSYS, end of the attachment beams were clamped to represent the substrate and modal analysis has been done. Fig. 4.2 illustrates the stress distribution of the system in the length extensional mode. Fig. 4.2(a) shows the stress distribution in the x direction. The attachment beams are stress free for x directed stress waves. Fig. 4.2(b) shows the stress distribution in the y direction. In this case, stress waves propagate through the substrate which cause the anchor loss.

4.2.1 Anchor Loss Calculation

The main cause of the anchor loss for this resonator type is the nonzero *Poisson's ratio.* As the resonator vibrates in the x direction, center region is maximally

stressed. This stress results sinusoidal expanding and contracting in the y direction depending on the Poisson's ratio. Hence, the attachment beams which are directly connected to the substrate, are excited to vibrate in the extensional mode. The stress waves reaching to the anchor points cause the substrate (anchor) loss. Analytical details of the substrate loss will be given in this section. The perturbation method used in [41] for the analysis of microdisk resonators will be used for the structure in Fig. 4.1. The main steps to find the anchor loss are the following. First, the mode shape and stress distribution of the resonator will be found as if it vibrates freely in air without the attachment beams. The transverse vibration displacement of the resonator due to Poisson effect will be calculated, this excites the attachment beams in longitudinal vibration. Vibration of the attachment beams result stress waves at the clamped regions that result the anchor loss.

The bar with length $2L$ can be analyzed by dividing it into two parts with length L which equals $\lambda/4$ at the resonance frequency. The wave equation along the resonator is

$$c_0^2 \frac{\partial^2 u(x,t)}{\partial^2 x} = \frac{\partial^2 u(x,t)}{\partial^2 t} \tag{4.1}$$

where $u(x,t)$ is the displacement in the x direction and c_0 is the wave speed. With a harmonic time dependance such that $u(x,t) = U(x)e^{jwt}$ Eq. 4.1 becomes

$$\frac{\partial^2 U(x)}{\partial^2 x} + \frac{w^2}{c_0^2} U(x) = 0 \tag{4.2}$$

Solving the equation with the boundary condition that, at $x = 0$ displacement is zero, $U(x)$ equals

$$U(x) = Asin\frac{2\pi x}{\lambda} \tag{4.3}$$

where A is the amplitude of the displacement and λ is the wavelength which equals $2\pi c_0/w$. The stored energy of the resonator with length L can be found by integrating the maximum kinetic energy along the x direction.

$$W_1 = \int_0^L \frac{1}{2} w^2 U(x)^2 dM = \frac{A^2 w^2 \rho L h t}{4} \tag{4.4}$$

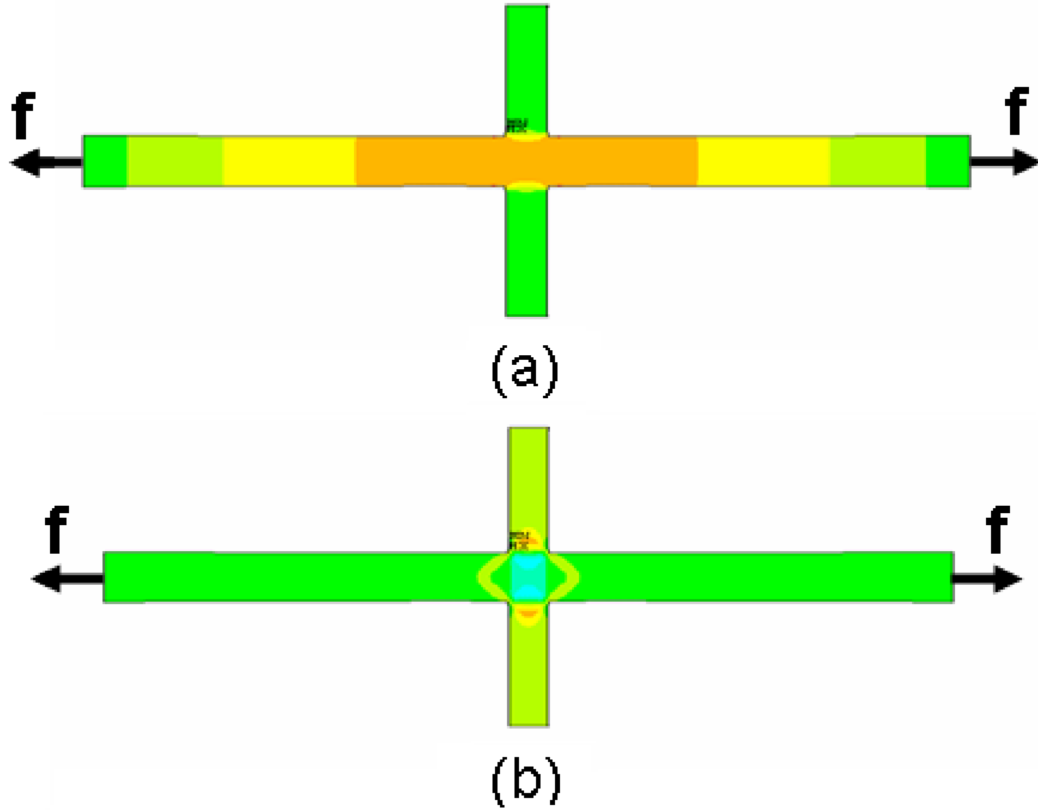

Figure 4.2: Mode shape and stress distribution of a length extensional mode resonator. (a) Stress in the longitudinal,x, direction, (b) Stress in the transverse,y, direction. Green regions show the stress free regions. Stress is larger at the regions shown with darker colors.

where ρ is the material density t and h are the thickness and width of the resonator respectively.

The stress wave along the resonator equals the Young's modulus (E) times the derivative of the displacement with respect to x.

$$P(x) = E\frac{\partial U(x)}{\partial x} = EA\frac{2\pi}{\lambda}\cos\frac{2\pi x}{\lambda} \tag{4.5}$$

Stress in the x direction results in a strain in the y direction, $\varepsilon_y(x)$, depending on the Poisson's ratio and Young's modulus.

$$\varepsilon_y(x) = \frac{-\nu P(x)}{E} \tag{4.6}$$

So, the displacement in the transverse direction equals

$$A_y(x) = \varepsilon_y(x)h/2 \tag{4.7}$$

This is the amplitude of the vibration of the attachment beam at $y = a$. Eq. 4.7 results an amplitude changing in the x direction. If the width of the attachment beams b is chosen to be much smaller than L, $A_y(x) = A_y(0)$ approximation can be valid. A more accurate approximation would be averaging $A_y(x)$ between $-b/2 < x < b/2$. After this averaging operation, uniform displacement amplitude of the attachment beam equals

$$A_1 = -\frac{1}{b}\int_{-b/2}^{b/2} \frac{\pi\nu Ah}{\lambda}\cos\frac{2\pi x}{\lambda}dx \;\; = \frac{\nu hA}{b}\sin(\frac{\pi b}{\lambda}) \tag{4.8}$$

Displacement along the attachment beam in the y direction can be found by solving the wave equation (Eq. 4.2) in the y direction with the boundary condition that $U_y(0) = 0$.

$$U_y(y) = U_o \sin(\frac{2\pi y}{\lambda}) \tag{4.9}$$

At $y = a$, $U_y(y)$ equals A_1, so we get

$$U_0 = \frac{A_1}{\sin(\frac{2\pi a}{\lambda})} \tag{4.10}$$

Stress wave along the attachment beam in the y direction can be found similarly with the Eq. 4.5.

$$P_y(y) = EU_0\frac{2\pi}{\lambda}\cos\frac{2\pi y}{\lambda} \tag{4.11}$$

So, the uniform stress at $y = 0$ equals

$$\sigma_y = EU_0\frac{2\pi}{\lambda} \tag{4.12}$$

Anchor loss due to normal stress source σ_y at the clamped region can be found using the equations in [40]. We have used the equation derived for circular cross sections and modified it such that the same stress source causes same amount of loss for equal areas of circular or rectangular clamped regions. The reason behind this preference is that the formulas for circular clamped regions have

been in agreement with experiments and our FEM simulations. With this in mind the anchor loss equals

$$W_{loss} = \frac{\sigma^2 b^2 t^2 w \gamma F(\gamma)}{2\rho c_t^3} \tag{4.13}$$

where

$$c_t = \sqrt{\frac{E}{2\rho(1+\nu)}} \tag{4.14}$$

$$\gamma = \sqrt{\frac{2(1-\nu)}{1-2\nu}} \tag{4.15}$$

$F(\gamma)$ is given by the imaginary part of an integral [40]

$$F(\gamma) = Im \int_0^\infty \frac{\zeta\sqrt{\zeta^2-1}}{\left(\gamma^2-2\zeta^2\right)^2 - 4\zeta^2\sqrt{\zeta^2-\gamma^2}\sqrt{\zeta^2-1}} d\zeta \tag{4.16}$$

Quality factor equals 2π times the ratio of the total stored energy over total lost energy. Total stored energy should also include the energy in the attachment beam which can be found by Eq. 4.4;

$$W_2 = \frac{w^2 U_0^2 \rho b t}{4}\ (a + \frac{\lambda}{4\pi} sin \frac{4\pi a}{\lambda}) \tag{4.17}$$

So, combining Eqs. 4.4, 4.13 and 4.17, quality factor due to anchor loss can be found as

$$Q = 2\pi\ \frac{W_1 + W_2}{W_{loss}} \tag{4.18}$$

4.2.2 Small Signal Electrical Equivalent Circuit

An electrical equivalent circuit can be constructed to calculate the quality factor of the resonator in the Fig. 4.1 similar to the one in the previous chapter. Difference from the circuits in the Chapter III is that for this case an electrical device is required to model the relationship between the stress at the center of the resonator to the velocity at the tip of the attachment beams. (i.e the relation between $P(x)$ in Eq. 4.5 and $wA_y(x)$ in Eq. 4.7 around $x = 0$). Hence the device should provide the relation between the voltage at one port to the current at the

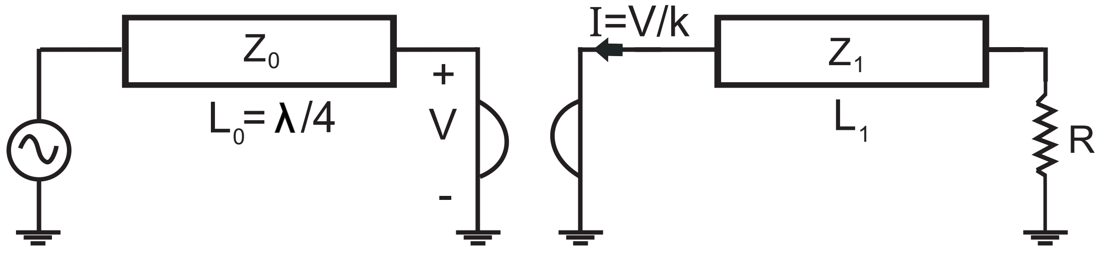

Figure 4.3: Equivalent electrical circuit of the resonator in the fig. 4.1. One half of the resonator is modeled since the resonator is perfectly symmetric. The gyrator has a ratio of k.

other port (Force-Voltage, Velocity-Current analogy given in the table 2.1). This can be achieved with a gyrator. Fig. 4.3 shows the electrical equivalent circuit of the resonator in Fig. 4.1. The circuit models one part of the resonator as the other part is perfectly symmetric. The transmission line with characteristic impedance Z_0 models the resonator with length L which equals $\lambda/4$ at resonance. The voltage at the end of the transmission line is the input to the first port of the gyrator. The gyrator converts this voltage to a current at the second port with a value of V/k where k is the ratio constant of the gyrator. The current excites the TL with the characteristic impedance of Z_1 which models the attachment beam. The termination resistance R models the substrate. Values of Z_0, Z_1 and R can be found by Eqs. 3.8 and 3.17. The k value can be extracted from Eqs. 4.5, 4.6 and 4.7.

$$k = \frac{V}{I} = \frac{P(x)ht}{-wA_y(x)} = \frac{2Et}{\nu w} \tag{4.19}$$

The equivalent circuit is fairly intuitive. The gyrator functions as an impedance inverter. The high impedance of the substrate is converted to a lower impedance by a transmission line (attachment beam), the gyrator re-inverts this impedance to a high value at the load of the first transmission line which is crucial to obtain a high-Q quarter wavelength resonator. The circuit was simulated in an electrical simulator, Q values extracted from the electrical circuit are consistent with Eq. 4.18.

In the work of Matilla et. al [5] a Q value of 180,000 was obtained for the dimensions $L = 180\mu m$, $h = 10\mu m$, $t = 8\mu m$, $a = 40\mu m$ and $b = 8\mu m$. For this resonator the analytical calculations expressed above and the equivalent circuit predicts a Q of 680,000. The mismatch between the calculations and the experiment can be attributed to several factors. The calculations and the equivalent circuit assumes a perfectly symmetric structure, however due to lithographic resolution, asymmetries are not avoidable which can cause flexural motions of the attachment beams and decrease Q. Another loss mechanism other than anchor loss might have been responsible for the difference.

Examining the equivalent circuit (Fig. 4.3) reveals that to maximize the Q value, the length of the attachment beam should be equal to $\lambda/4$. If $a = 180\mu m$ instead of $40\mu m$ had been used in [5], an order of increase in Q value would result. This is also clarified in Eq. 4.10, when $a = \lambda/4$, $U_0 = A_1$; when $a = 40\mu m = \lambda/18$, $U_0 = 2.9A_1$, therefore for the latter case the lost energy is 8.5 times larger.

The design can be improved more for higher frequency applications as the anchor loss greatly increases at high frequencies. The idea presented in Chapter-III can be adopted to decrease the resistance seen by the gyrator by adding area mismatched beams. Fig. 4.4 illustrates such a structure, $\lambda/4$ length three beams are used to decrease the high resistance of the substrate to a much smaller value.

4.3 Filter Design

Mechanical filters have been widely used in the electronic circuits since the Q of the electrical components are not adequate to obtain the desired signal selectivity. History of the electromechanical filters dates back to 1940s [43], [44]. The basic method for constructing electromechanical filters is coupling high-Q resonators to obtain a desired bandwidth with a specific band shape. Electromechanical

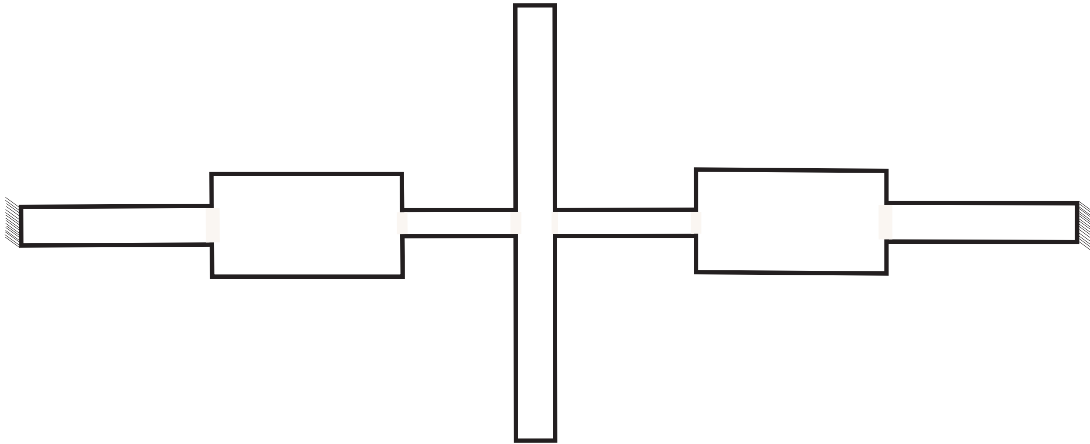

Figure 4.4: Length extensional mode resonator improved with area mismatched attachment beams.

filters function by converting the electrical signal to a mechanical signal and processing it by High-Q mechanical processors and converting it back to the electrical domain.

SAW, crystal, ceramic filters are widely used in high frequency applications. However these components are off-chip parts hence they span too much area, cost much and can not benefit the advantages of being integrated with IC as reducing the parasitic effects. To avoid the disadvantages of the off-chip counterparts, micromechanical filters fabricated with IC compatible techniques have been proposed [45]. The first example is the resonant gate transistor [2], introduced by Nathanson et al. in 1967. It is based on the vibration of the gate of a field effect transistor. The characteristics of the resonant gate transistor was not satisfactory ($Q \approx 90$) however fundamentals of micromechanical filters have been established with the work. Recently, great improvements have been in the design of micromechanical resonators and filters. Q values, temperature stability and aging characteristic of these devices are fairly promising to replace the macroscopic mechanical counterparts [19].

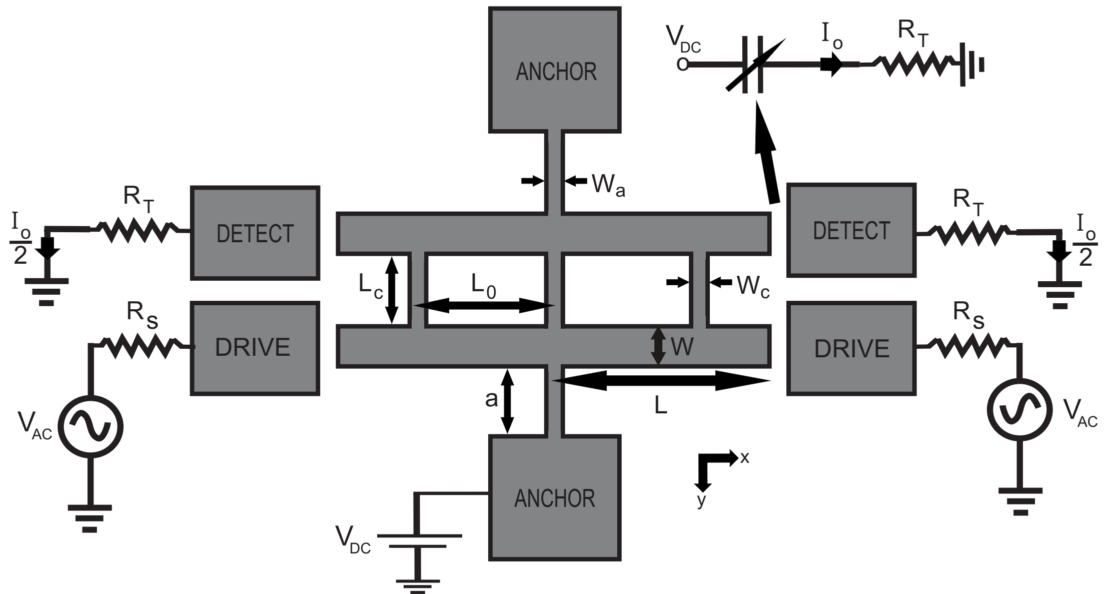

Figure 4.5: Proposed filter type with excitation and detection electronics.

In principle, similar to the electronic filters, mechanical filters are constructed by coupling high Q resonator blocks with electrical or mechanical coupling elements. The center frequency of the filter is determined by the resonance frequency of the identical resonators and the bandwidth is determined by the coupling elements. There are huge number of resources and tools to implement ladder type (Butterworth, Chebyshev, Elliptical etc.) electronic filters which can be adopted to the mechanical domain. Design steps to obtain specific micromechanical filter characteristics have been presented in several publications [45], [46]. Working principle of these structures are based on mode splitting explained in the Chapter II.

In this section, a new micromechanical filter suitable for IC integration is proposed. The filter is composed of two rectangular resonators to vibrate in the length extensional mode and they are coupled with symmetrically located beams. Fig. 4.5 illustrates the proposed filter type with the excitation and detection electronics. A *DC* voltage is applied to the main body which is composed of a conductive material such as doped silicon. The first rectangular resonator (in

the lower part of the structure) is vibrated symmetrically by applying an AC voltage to the drive electrodes which results a force component at the resonance frequency given by:

$$F = \frac{V_{DC} V_{AC} C_0}{d_0} \tag{4.20}$$

C_0 and d_0 are the static capacitance and the gap distance between the drive electrodes and resonator, derivation of the force equation is explained in the Chapter-II. The displacement of the first resonator can be found using Eq. 2.8 which equals $X = FQ/k_r$ at resonance. Q and k_r are the quality factor and the stiffness of the resonator. X is the displacement at the tip point of the first resonator and it is transformed to the coupling beams depending on the ratio of L_0/L. L and L_0 are the half length of the first resonator and the distance of the coupling beam to the center, the dimensions are shown in the figure 4.5. The displacement at the other ends of the coupling beams depend on the $ABCD$ matrices of the beams which will be explained in the next section. Second resonator is vibrated by the excitation of the coupling beams and a time varying capacitance is formed between the resonator and the detection electrodes. The DC biased, time varying capacitance results the filtered output current.

$$I_0 = \frac{\partial C(x,t) V_C}{\partial t} = V_{DC} \frac{\partial C(x,t)}{\partial x} \frac{\partial x}{\partial t} \tag{4.21}$$

4.3.1 Coupling Beam Design

The filter characteristic is the result of two closely spaced modes which are shown in Fig. 4.6, Chapter-II includes more detail on mode splitting. The symmetric mode (Fig. 4.6-a) comes out at the resonance frequency of a single length extensional mode rectangular block. The frequency of the anti-symmetric mode is slightly higher than the symmetric mode and it is determined by the frequency of the symmetric mode and the coupling beams. The spacing between the two

modes determines the bandwidth therefore design of the coupling beams is the main step to specify the filter's output response. Bandwidth is proportional to the ratio between the spring constant of the coupling beam and the resonator. This is clarified by Eq. 2.39.

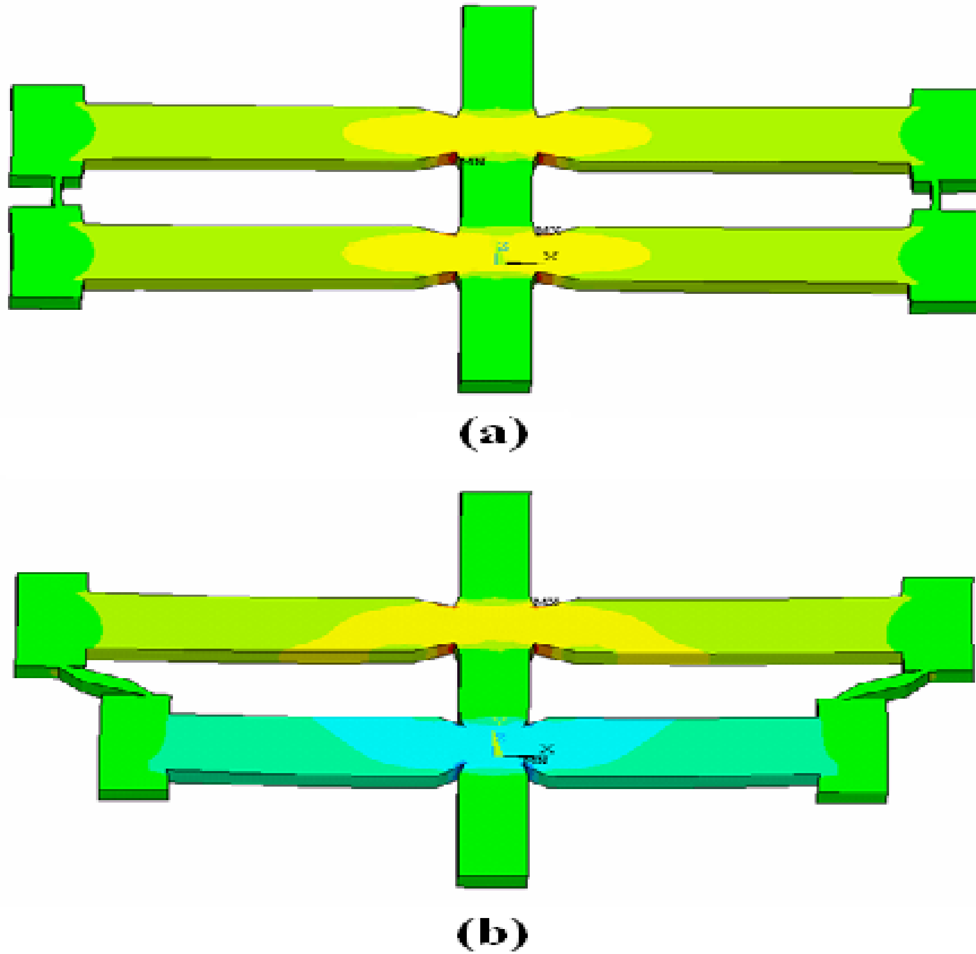

Figure 4.6: Mode shapes and stress distribution of the filter.(a) In symmetric mode, both resonators vibrate in phase. (b) In anti-symmetric mode the resonators vibrate with a phase difference of 180°.

$$B \propto \frac{k_c}{k_r} \tag{4.22}$$

To design a filter with a narrow bandwidth, spring constant of the coupling beams should be made small relative to the spring constant of the resonator. This can be achieved in two ways: Geometry of the coupling beam can be modified to reduce k_c, i.e. narrower and longer beams can be used. The second method

is based on the location of the coupling beam. Connecting the beams to the low velocity points of the resonators reduces the coupling and bandwidth, because k_r is effectively larger at those locations. In other words bandwidth is proportional to the L_0/L ratio. Hence locating the coupling beams away from the tip point of the resonators will results filters with narrower bandwidths. Low velocity coupling is very advantageous as the width of the coupling beams is constraint by the lithographic limits.

4.3.2 Two Port Representation of the Coupling Beams

Fig. 4.7(a) illustrates the shapes of the coupling beam during vibration. While the rectangular blocks resonate in the length-extensional mode, coupling beams vibrate in the flexural mode. Analysis of the beams are based on Euler-Bernoulli equations. Impedance matrices have been constructed by extracting the two port characteristics of the flexural mode beams in [47]. The analysis are based on finding the $ABCD$ matrices relating the force and velocity at one port of the system to the force and velocity at the other port. This section will not cover the detailed analysis instead the results presented in [47] and [45] will be given directly. For the case in the fig. 4.7, rotation angles at the ends of the flexural coupling beam equal zero, then the $ABCD$ matrix equals [45]

$$\begin{bmatrix} F_1 \\ V_1 \end{bmatrix} = \begin{bmatrix} H_6/H_7 & j2KH_1/H_7 \\ -jH_3/(KH_7) & H_6/H_7 \end{bmatrix} \begin{bmatrix} F_2 \\ V_2 \end{bmatrix} \tag{4.23}$$

F_n and V_n are the force and velocity at port n, shown in Fig. 4.7(b). Where

$$H_1 = \sinh(\alpha)\sin(\alpha) \tag{4.24}$$

$$H_3 = \cosh(\alpha)\cos(\alpha) - 1 \tag{4.25}$$

$$H_6 = \sinh(\alpha)\cos(\alpha) + \cosh(\alpha)\sin(\alpha) \tag{4.26}$$

$$H_7 = \sinh(\alpha) + \sin(\alpha) \tag{4.27}$$

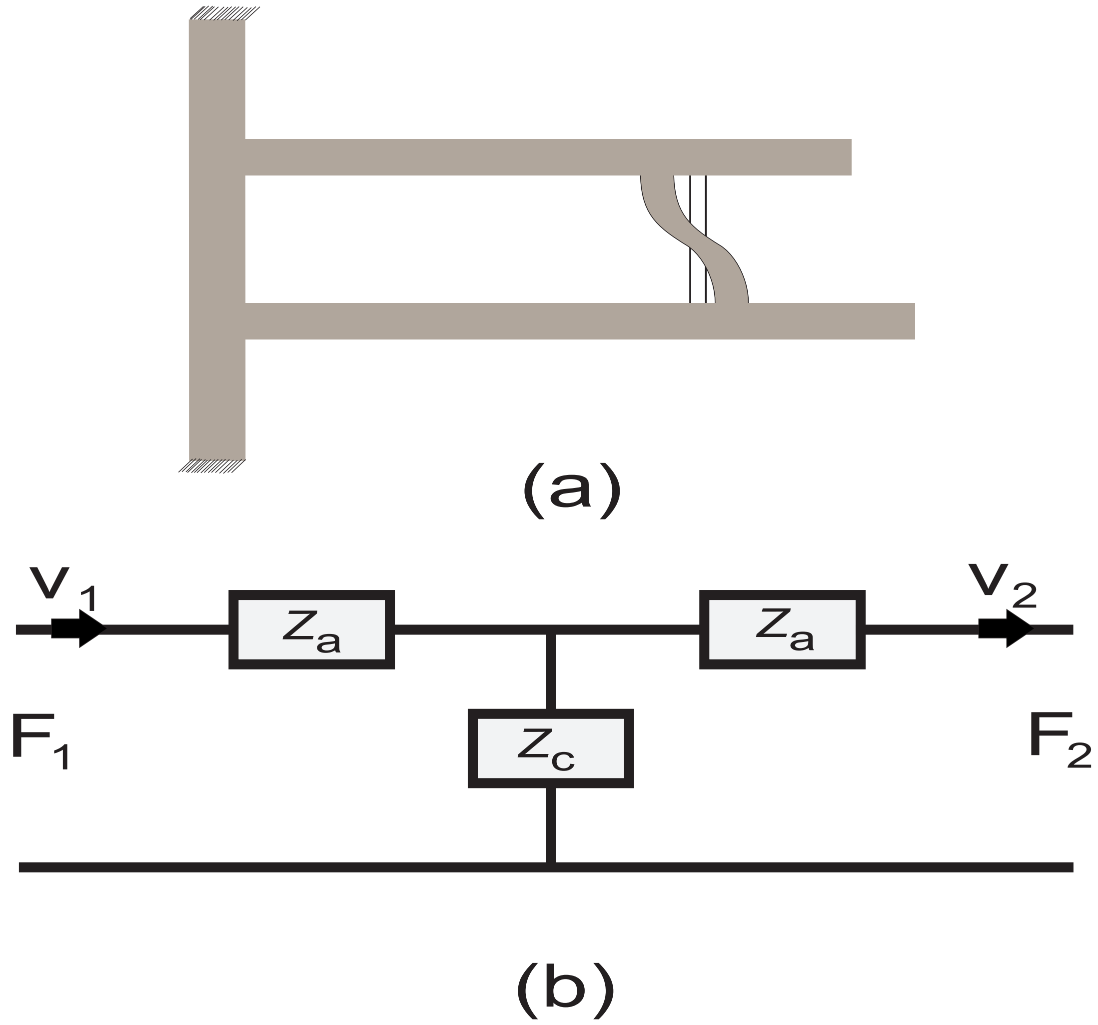

Figure 4.7: (a) Vibration shape of the coupling beam, the coupling beam is in flexural motion while the resonators vibrate in the elongation mode. (b) Equivalent two port representation of the coupling beams

$$\alpha = [(\rho t W_c / EI) w^2 L_c^4]^{1/4} \tag{4.28}$$

$$I = t W_c^3 / 12 \tag{4.29}$$

$$K = EI\alpha^3 / (w L_c^3) \tag{4.30}$$

W_c, t, L_c are the width, thickness and length of the beam. E and ρ are the Young's modulus and the density of the beam material. For this $ABCD$ matrix (Eq. 4.23), $AD - BC = 1$ which is required for a reciprocal structure [36]. Fig. 4.7(b) illustrates the two port representation of the coupling beam. The

impedance values can be found by transforming the $ABCD$ matrix to a Z matrix form and equating it to the Z matrix of the two port in Fig. 4.7(b)

$$Z_a = \frac{jK(H_6 - H_7)}{H_3} \tag{4.31}$$

$$Z_c = \frac{jKH_7}{H_3} \tag{4.32}$$

For a two port as in the Fig. 4.7(b), when $Z_a = jX$ and $Z_c = -jX$, a load impedance of Z_L is converted to the impedance $Z = X^2/Z_L$ at the other port. This is the function of a quarter wavelength transmission line. Examining the equations 4.31 and 4.32, this condition holds when H_6 equals 0

$$H_6 = \sinh(\alpha)\cos(\alpha) + \cosh(\alpha)\sin(\alpha) = 0 \tag{4.33}$$

Choosing the dimensions of the coupling beams to make $H_6 = 0$, the beam can be modeled as an impedance inverter. Hence, in an equivalent circuit the coupling beam can be modeled with a T network consisting of two inductors and a capacitor (or vice versa) with impedance values of Z_a and Z_c.

4.3.3 Small Signal Equivalent Circuit of The Filter

The electrical equivalent circuit of the filter in Fig. 4.5 is shown in the Fig. 4.8. One part of the mechanical system is modeled as the other part is perfectly symmetric, i.e. the part shown in Fig. 4.7(a) is modeled. The resonator blocks are represented with RLC tanks as explained in the second chapter. m, k_r, b stand for the equivalent mass, stiffness and damping coefficient of the resonators.

The displacement function of the length extensional mode resonator has been derived previously, $U(x) = \sin\frac{2\pi x}{\lambda}$ (Eq. 4.3). and the resonance occurs at the frequency $L = \lambda/4$.

$$w_0 = 2\pi\frac{1}{4L}\sqrt{\frac{E}{\rho}} \tag{4.34}$$

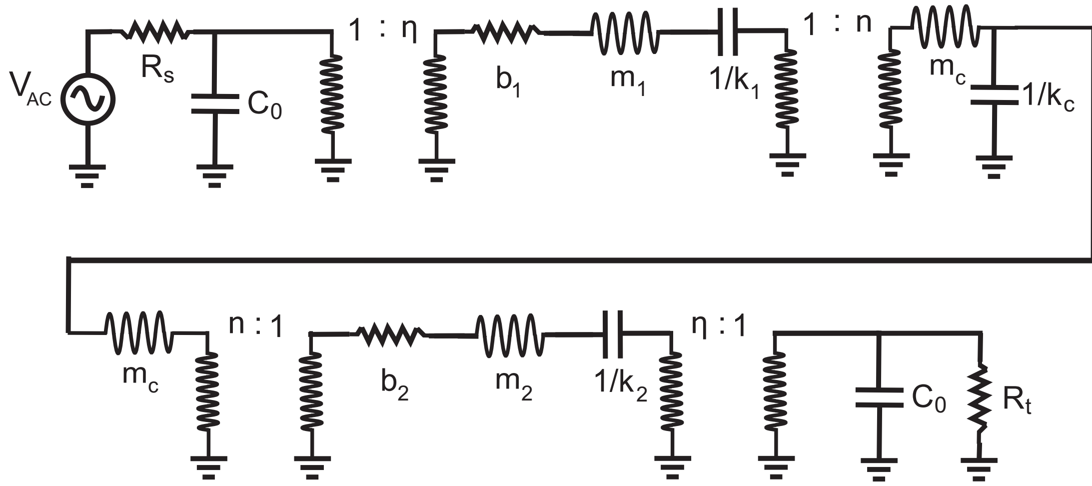

Figure 4.8: The electrical equivalent circuit of the filter in the figure 4.5.

Equivalent mass can be found by integrating the maximum kinetic energy along the beam and equating this energy to the kinetic energy of a concentric mass. By Eqs. 4.3 and 2.10 effective mass is found to be one half of the static mass.

$$m = \frac{1}{2}\rho LWt \tag{4.35}$$

W and t are the width and the thickness of the quarter-wave length resonator. k_r equals mw_0^2:

$$k_r = \frac{\pi^2}{8}\frac{EWt}{L} \tag{4.36}$$

which differs from the static spring constant with a ratio of $\pi^2/8$. The damping coefficient b equals mw_0/Q where Q is the quality factor of the resonator. Q can be found using the equivalent circuit shown in the Fig. 4.3. A first order approximation estimates a Q value of twice the one found by the circuit in Fig. 4.3. The reason is that the number of energy storage elements is doubled in the filter structure whereas there are still two paths towards the anchor points.

In Fig. 4.8, R_s and R_t are the source and the termination resistors. $C_0 = \epsilon_0 Wt/d_0$ is the static capacitance between the drive-sense electrodes and the coupled resonator structure. The transformers with the ratio $1:\eta$ has been

explained in the Chapter-II.

$$\eta = \frac{V_{DC}C_0}{d_0} \tag{4.37}$$

The transformers with the ratio $1 : n$ represent the velocity transformation from the resonators to the coupling beam. The n value depends on the location of the coupling beams. It equals inverse of the velocity ratio between the coupling beam location and the tip point of the resonator. Using Eq. 4.3:

$$n = [\sin(\frac{\pi}{2}\frac{L_0}{L})]^{-1} \tag{4.38}$$

If the coupling beams are attached to the maximum velocity points ($L_0 = L$), n equals 1. In the equivalent circuit, the coupling beams is modeled as a T network with components $m_c, 1/k_c, m_c$ values of which can be found by Eqs. 4.31 and 4.32. As transformer ratios η depend on V_{DC}, when V_{DC} equals zero, η equals zero and the device is off. Hence the DC bias can be used as a switching tool.

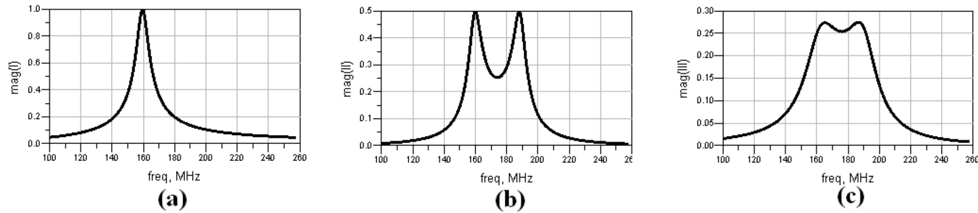

Figure 4.9: (a) Transfer function of a single resonator. (b) Transfer function of a coupled two resonator system. (c) The coupled resonator system is terminated with resistors to obtain a flat filter characteristic.

The response of coupled resonator system is composed of peaks in the band which should be avoided for a filter characteristics. To eliminate the peaks, proper termination resistances R_s and R_t should be used in the filter ends. Fig. 4.9(a) is the response of the single resonator, when the two resonators are coupled the transfer function becomes as in Fig. 4.9(b) due to the mode splitting

effect explained in the Chapter-II. The resistors R_s and R_t reduces the quality factor of the overall system and the peaks are avoided as shown in Fig. 4.9(c).

4.3.4 Filter Design Example and Simulation Results

In this section, design steps of a high-Q micromechanical filter to be operated at 100MHz will be presented. Length of the resonators have been fixed by determining the resonance frequency. For a silicon structure ($E = 150GPa$, $\rho = 2330kg/m^3$, $\nu = 0.3$), $L \approx 20\mu m$ satisfies the frequency requirement. Width and thickness of the resonators should be chosen concerning several factors as the electrostatic coupling efficiency which will determine the motional resistance, the potential spurious responses, quality factor and power handling capability etc. In this example, $W = 8\mu m$ and $t = 4\mu m$ has been chosen. For maximizing the quality factor, lengths of the attachment beams should also equal quarter wavelength ($a = 20\mu m$). Width of the attachment beams should be minimized to increase Q, $W_a = 3\mu m$ for this design. With these dimensions quality factor of the rectangular resonator blocks is around 30,000 (Anchor loss dominated condition is assumed). The Q factor is approximately twice the value that can be extracted from the equivalent circuit in the Fig. 4.3. As explained previously, this is the result of doubling the energy storage elements.

Having designed the high-Q blocks, next step is to design the coupling beams. A value of α that will satisfy the equation 4.33 should be determined. $\alpha = 3\pi/4 + m\pi$ are the solutions of equation 4.33, where m is an integer.

W_c and L_c, width and the length of the coupling beams should be determined concerning the bandwidth of the filter. For a narrow band response $W_c = 1\mu m$, typical lithographical limit is chosen. Eq. 4.28 reveals the parameters determining α. Apart from L_c, all other parameters have been chosen. Eq. 4.28 results $L_c = 1.91\ 10^{-6}\alpha$. As α can take infinitely many values there are infinitely many

choices of L_c. However the length of the coupling beams should not be too long, otherwise spurious modes of the coupling beams can be excited in the desired filter band. To decrease the bandwidth of the filter L_c should be maximized. Between the two boundaries, in this design we choose $L_c = 10.5\mu m$. Another dimension determining the bandwidth of the filter is the L_0 value. We have chosen $L_0 = 1.5\mu m$ in this design to minimize the bandwidth.

The filter dimensions have been determined, two other parameters d_0 and V_{DC} are required to calculate the values of the components in the equivalent circuit. In the calculations the static capacitive gap distance $d_0 = 100nm$ has been used which is a typical distance in the current filter fabrication processes. $V_{DC} = 10V$ bias voltage was assumed. Table 4.1 lists the design parameters and Table 4.2 lists the values of the components in the equivalent circuit.

Table 4.1: Dimensional and Technological Parameters of the Sample Filter

Parameter	*Value*	*Definition*
f_0	100 MHz	Resonance Frequency
L	$20\mu m$	Resonator Length
W	$8\mu m$	Resonator Width
a	$20\mu m$	Length of attachment beams
W_a	$3\mu m$	Width of attachment beams
t	$4\mu m$	Thickness
W_c	$1\mu m$	Width of the coupling beam
L_c	$10.5\mu m$	Length of coupling beam
L_0	$1.5\mu m$	Distance of coupling beam
d_0	$100nm$	Capacitive gap distance
V_{DC}	$10V$	DC Bias voltage

The electrical equivalent circuit in Fig. 4.8 has been simulated in a circuit simulator [1] with the parameters listed in tables 4.1 and 4.2. Fig. 4.10(a) illustrates the filter response when the output is terminated with a matched resistor. The value of the termination resistance equals twice the value of the motional resistance as there are two resonators. Motional resistance which equals $R_m = b/\eta^2$

[1]Advanced Design System, Agilent

Table 4.2: Component values of the equivalent circuit based on the values in Table 4.1

Parameter	*Value*	*Definition*
C_0	$2.82fF$	Static Capacitance
η	$2.82\ 10^{-7}$	Electromechanical Transformer Ratio
m	$7.45\ 10^{-13}\ kg$	Mass of the resonator
k_r	$296{,}000N/m$	Stiffness of the resonator
$1/k_r$	$3.37\mu F$	Capacitance
b	$1.56\ 10^{-8}\ kg/sec$	Damping Factor
R_m	$196k\Omega$	Motional Resistance
n	8.51	Coupling beam transformer ratio
Z_a	$-1.6\ 10^{-5}j$	Series Impedance in the T network
Z_c	$1.6\ 10^{-5}j$	Shunt Impedance in the T network
R_s	50Ω	Source Resistance
R_T	$392\ k\Omega{=}2R_m$	Termination Resistance

has been explained in detail in Chapter-II. The first peak in the filter response (at $\approx 100.42MHz$) is slightly higher than the resonance frequency of the rectangular blocks (at $\approx 100.29MHz$), this is due to the additional series impedances of the coupling beams. The selectivity of the filter can be increased by increasing the order i.e. the number of coupled resonators.

Fig. 4.10(b) illustrates the severely attenuated filter response when the output is terminated with a traditional 50 Ω resistor. High insertion loss results despite the high Q factor of the resonators, because of the mismatch between the motional resistance and the 50 Ω termination. Techniques to reduce the motional resistance has been explained in the Chapter-II. Another solution might be changing the 50 Ω tradition to a higher value to benefit the advantageous of the micromechanical filters.

For a flat in-band response, the peaks can be avoided with proper termination resistances as explained in the figure 4.9. The termination resistances load the quality factor of the resonators and prevent the peaks caused by the high unloaded Q value of each resonators. To a first order approximation, the ratio of the termination resistances to the motional resistance of the resonators equal the

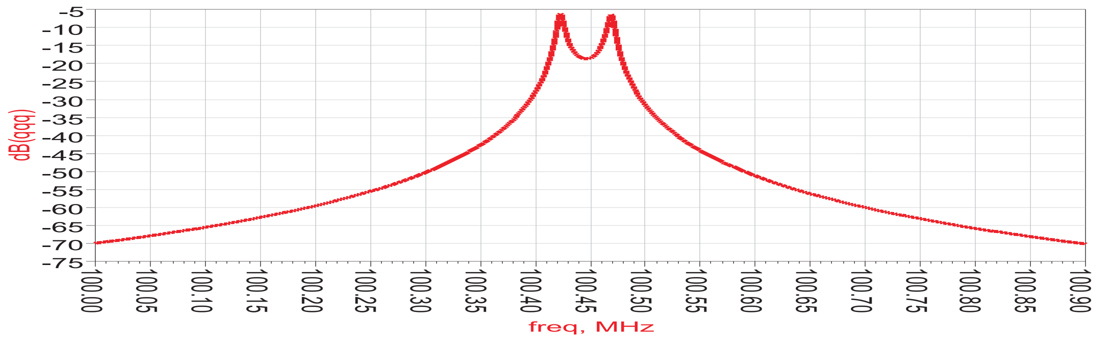

(a)

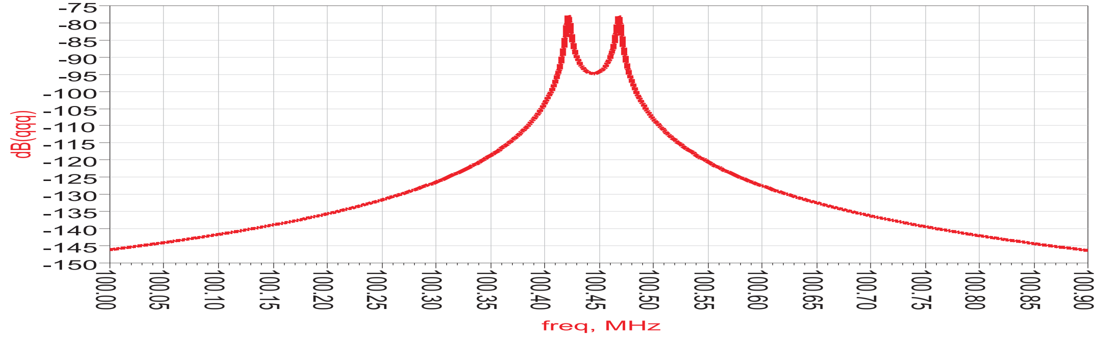

(b)

Figure 4.10: (a) Response of the filter design with parameters given in the tables 4.1, 4.2. (b) Response of the same filter, terminated with 50Ω.

ratio between the filter bandwidth and the bandwidth of the unloaded resonators. For this particular design example, choosing $R_t = R_s = 2500k\Omega$ avoids the peaks. The static capacitances C_0 undermines the effects of termination resistances as they are in parallel. C_0 capacitance can be tuned with an inductor which results other practical issues explained in [48]. The circuit has been terminated at both ends with tuned inductors to eliminate the effects of C_0. The flat response is shown in the figure 4.11. Implementing high-Q inductors at high frequencies is not practical therefore instead of tuning C_0 with an inductor, motional resistance of the resonators should be reduced which will directly reduce the value of the required termination resistances. Low motional resistances is crucial also for dynamic range purposes. Large thermal noise of the huge resistors will limit the dynamic range of the filter.

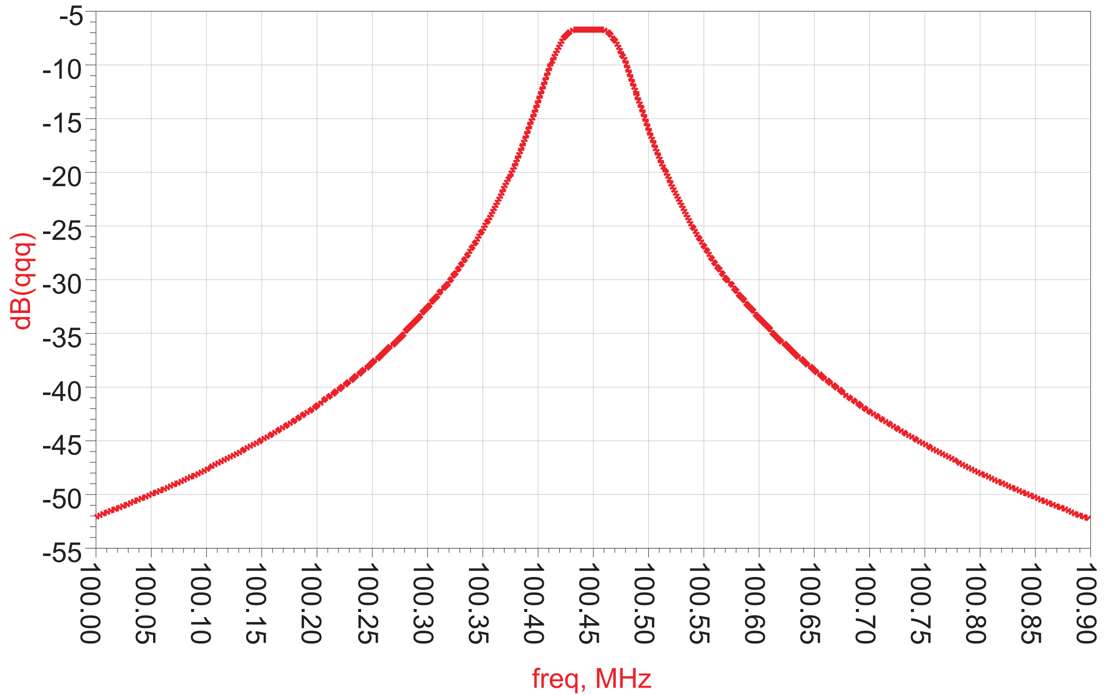

Figure 4.11: Flat filter response obtained with proper termination resistances

Selectivity of the filter can be enhanced by increasing the order of the filter. By coupling seven resonators, the electrical equivalent circuit expects the filter response shown in the figure 4.12. The filter was terminated with a matched resistance therefore the in-band peaks can be observed. The response is the result of seven modes which correspond to the respective peaks in the figure.

Fig. 4.13 shows the efficiency of the low velocity coupling. For this case, the distance of the coupling beams have been changed from $L_0 = 1.5\ \mu m$ to $L_0 = 5\ \mu m$. The resonance modes get apart and the in-band transmission reduces. Width of the coupling beams had already been chosen at the technological limit therefore low velocity coupling is a crucial tool to reduce the filter band.

In the equivalent circuit shown in Fig. 4.8, the parasitic effects have not been included. There are several parasitic effects that will degrade the performance of the filters. Fig. 4.14(a) shows a filter fabricated on a Silicon On Insulator (SOI) wafer. If the wafer is not grounded, there will be a direct path between the drive

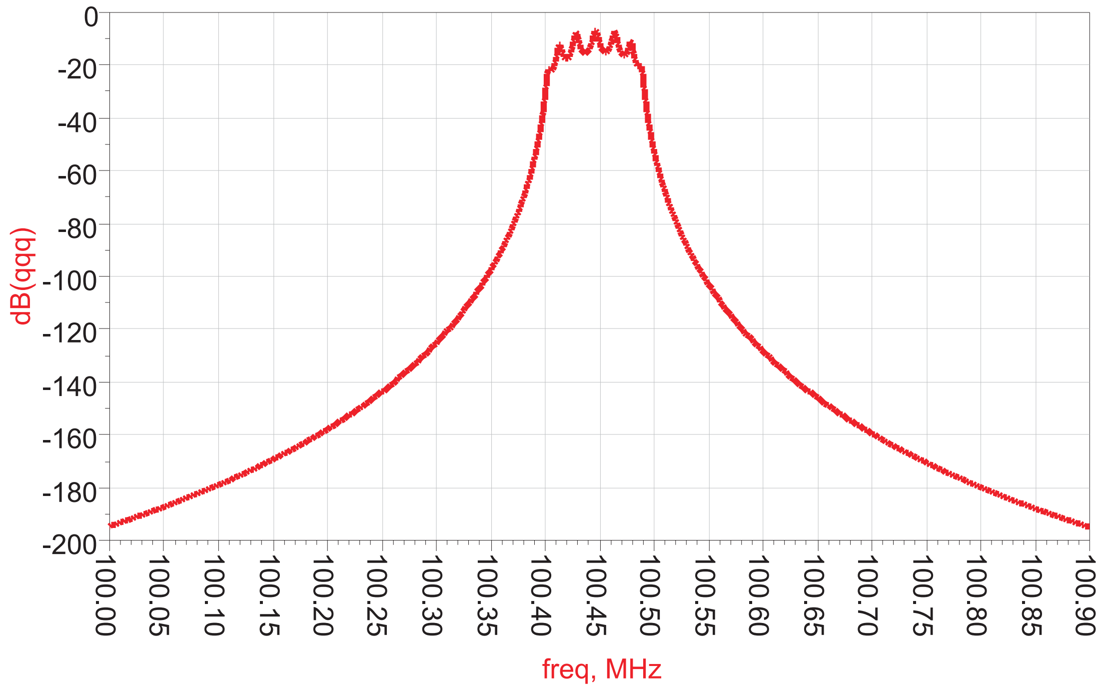

Figure 4.12: Response of a seventh order filter, compare with the response of the second order filter response shown in Fig. 4.10 (a).

and sense electrodes. Between the electrodes and the wafer, capacitors are formed by the oxide layer and these capacitances are connected through an equivalent resistor value of which depends on the conductivity of the wafer. Fig. 4.14(b) shows the modified equivalent circuit with the parasitic components. The modified circuit was simulated using typical dimensions of pads and wafer resistivity. Fig. 4.15 shows the degraded filter response by the parasitics. The selectivity of the filter has reduced significantly due to the background feedthrough signal. This parasitic effect can be avoided by grounding the substrate which breaks the feedthrough path. In [24] a doped layer has been formed within the substrate and the layer was grounded which eliminated the feedthrough current.

Recent developments in micromechanical filter designs have aimed to overcome the two main problems, large motional resistance and parasitic effects. To reduce the motional resistance down to 50 Ω, arraying techniques have been

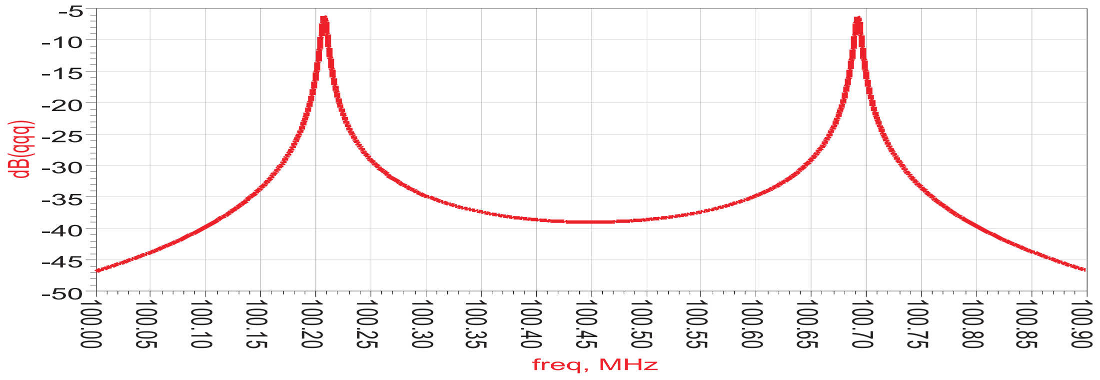

Figure 4.13: The filter response for L_0=5μm, the efficiency of the low velocity coupling can be examined by comparing with the response shown in the fig. 4.10 (a).

improved which are explained in the Chapter-II. Parasitic effects have been softened, by differential operation techniques in [49] and [11]. Fig. 4.16 illustrates a differential disk array filter design [11]. Li et. al. have arrayed microdisk resonators and the motional resistance reduced down to 977 Ω. By the differential operation the feedthrough floor was reduced around 20dB.

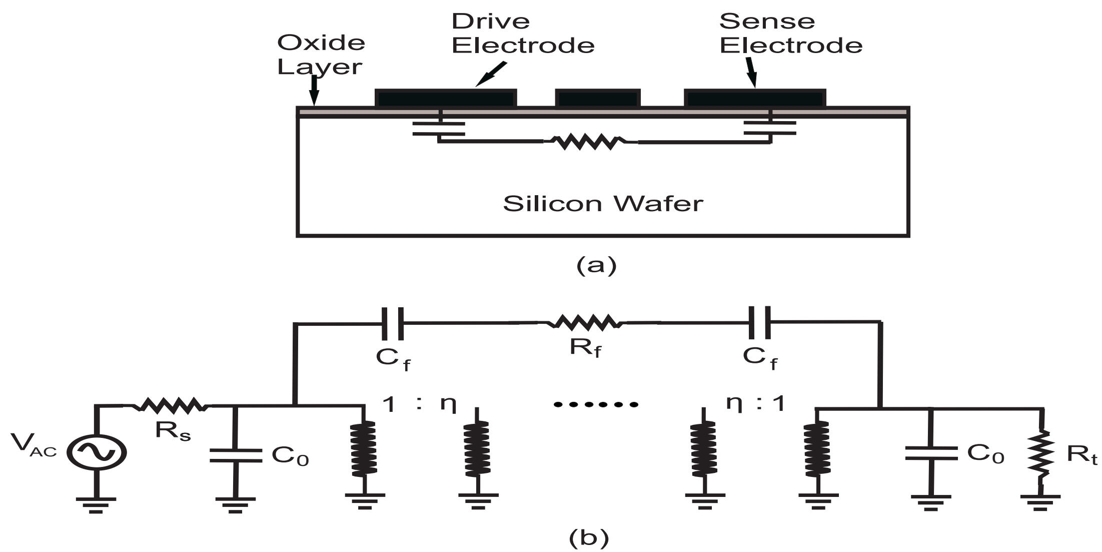

Figure 4.14: (a) Feedthrough path through the wafer. (b) The feedthrough parasitics in the equivalent circuit.

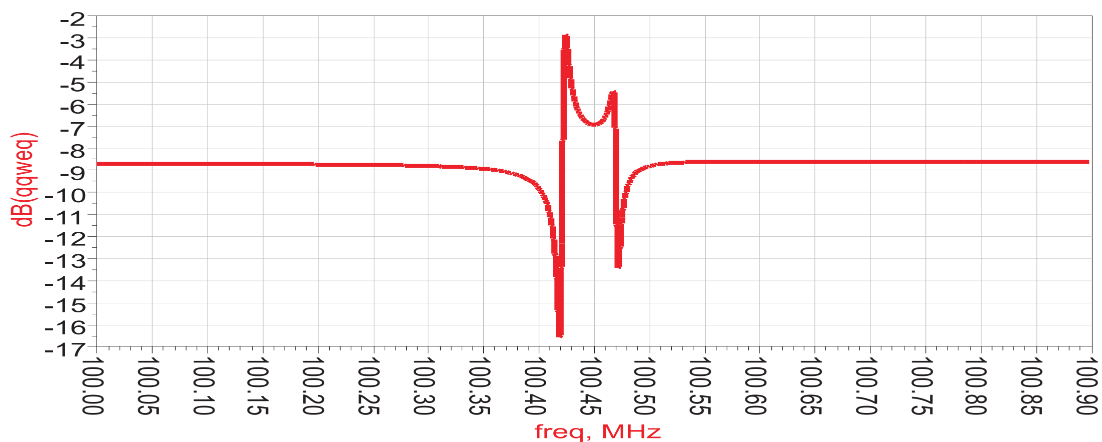

Figure 4.15: The filter response with the feedthrough parasitics. Compare with the response in Fig. 4.10 (a).

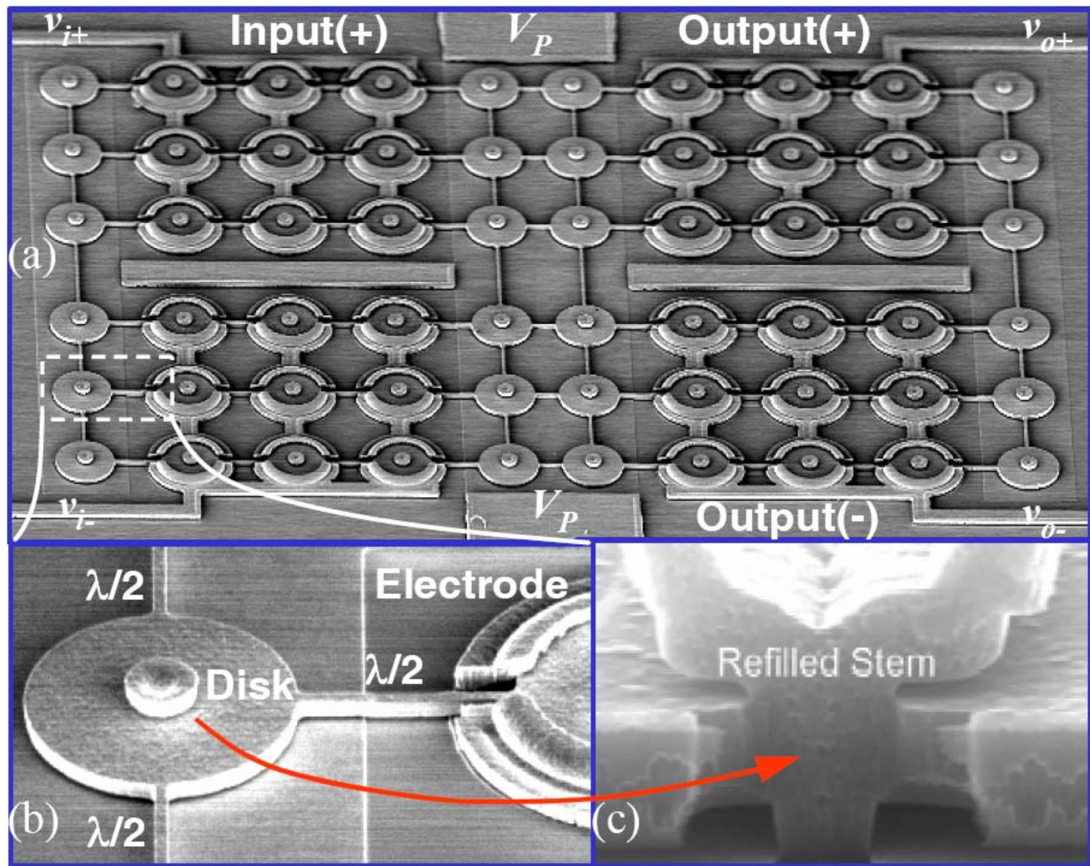

Figure 4.16: Medium Scale Integrated Differential Disk Array Filter [11].

Chapter 5

CONCLUSIONS

We have introduced a novel micromechanical resonator type. The FEM results are consistent with the theoretical calculations. The resonator type is advantageous in term of relatively easy fabrication processes with respect to the similar resonators. Performance of the state of the art radio frequency micromechanical resonators are generally limited by the anchor loss. Our solution to decrease the anchor loss is very promising to increase the performance of existing designs. Simulation results of the proposed micromechanical filters are optimistic since they rely on perfect symmetry. As the operation frequency increases, the length of the filter will decrease and the effect of lithographical uncertainties will increase. For more reliable results, the filters should be fabricated and practical limitations should be examined.

The future work will consist of fabrication and testing of the micromechanical resonator and the filter designs. An oscillator circuit will be implemented using the novel area mismatched resonator type. Future research will also focus on increasing the performance of the these devices. Methods will be searched to

enhance the electrostatic coupling efficiency in order to decrease the motional resistance down to 50Ω. Processes techniques to co-fabricate the micromechanical devices with integrated circuits will also be developed.

Bibliography

[1] C. T.-C. Nguyen, "Micromechanical RF Devices for Communication Transceivers." Transducers 01, Short Course, 2001.

[2] H. Nathanson, W. Newell, R. Wickstrom, and J. Davis, J.R., "The resonant gate transistor," *Electron Devices, IEEE Transactions on*, vol. 14, pp. 117–133, Mar 1967.

[3] C.-C. Nguyen and R. Howe, "Quality factor control for micromechanical resonators," pp. 505–508, Dec 1992.

[4] K. Wang, A.-C. Wong, and C.-C. Nguyen, "VHF free-free beam high-Q micromechanical resonators," *Microelectromechanical Systems, Journal of*, vol. 9, pp. 347–360, Sep 2000.

[5] T. Mattila, J. Kiihamäki, T. Lamminmäki, O. Jaakkola, P. Rantakari, A. Oja, H. Seppä, H. Kattelus, and I. Tittonen, "A 12 MHz micromechanical bulk acoustic mode oscillator," *Sensors and Actuators A: Physical*, vol. 101, no. 1–2, pp. 1–9, 2002.

[6] S. Pourkamali, Z. Hao, and F. Ayazi, "VHF single crystal silicon capacitive elliptic bulk-mode disk resonators-part II: implementation and characterization," *Microelectromechanical Systems, Journal of*, vol. 13, pp. 1054–1062, Dec. 2004.

[7] G. Piazza, P. Stephanou, J. Porter, M. Wijesundara, and A. Pisano, "Low motional resistance ring-shaped contour-mode aluminum nitride piezoelectric micromechanical resonators for UHF applications," pp. 20–23, Jan.-3 Feb. 2005.

[8] J. Wang, J. Butler, T. Feygelson, and C.-C. Nguyen, "1.51-GHz nanocrystalline diamond micromechanical disk resonator with material-mismatched isolating support," in *"17th IEEE Int. Conf. on Micro Electro Mechanical Systems"*, pp. 641–644, 2004.

[9] S.-S. Li, Y.-W. Lin, Y. Xie, Z. Ren, and C.-C. Nguyen, "Micromechanical "hollow-disk" ring resonators," in *"17th IEEE Int. Conf. on Micro Electro Mechanical Systems"*, pp. 821–824, 2004.

[10] W. Newell, "Face-mounted piezoelectric resonators," *Proc. of the IEEE*, vol. 53, pp. 575–581, June 1965.

[11] S.-S. Li, Y.-W. Lin, Z. Ren, and C.-C. Nguyen, "An MSI Micromechanical Differential Disk-Array Filter," pp. 307–311, June 2007.

[12] R. G. Kinsman, *Crystal filters: design, manufacture, and application.* New York, NY, USA: John Wiley & Sons, Inc., 1986.

[13] A. Bateman and D. Haines, "Direct conversion transceiver design for compact low-cost portable mobile radio terminals," pp. 57–62 vol.1, May 1989.

[14] P. Gray and R. Meyer, "Future directions in silicon ICs for RF personal communications," pp. 83–90, May 1995.

[15] L. Lin, R. Howe, and A. Pisano, "Microelectromechanical filters for signal processing," *Microelectromechanical Systems, Journal of*, vol. 7, pp. 286–294, Sep 1998.

[16] J. Clark, W.-T. Hsu, M. Abdelmoneum, and C.-C. Nguyen, "High-Q UHF micromechanical radial-contour mode disk resonators," *J. of Microelectromechanical Systems*, vol. 14, pp. 1298–1310, Dec. 2005.

[17] S. Pourkamali and F. Ayazi, "Electrically coupled MEMS bandpass filters: Part II. Without coupling element," *Sensors and Actuators A: Physical*, vol. 122, no. 2, pp. 317 – 325, 2005.

[18] Y.-W. Lin, S. Lee, S.-S. Li, Y. Xie, Z. Ren, and C.-C. Nguyen, "60-MHz wine-glass micromechanical-disk reference oscillator," pp. 322–530 Vol.1, Feb. 2004.

[19] C.-C. Nguyen, "MEMS technology for timing and frequency control," *Ultrasonics, Ferroelectrics and Frequency Control, IEEE Transactions on*, vol. 54, pp. 251–270, February 2007.

[20] S. Pourkamali, G. Ho, and F. Ayazi, "Vertical capacitive SiBARs," pp. 211–214, Jan.-3 Feb. 2005.

[21] K. Yasumura, T. Stowe, E. Chow, T. Pfafman, T. Kenny, B. Stipe, and D. Rugar, "Quality factors in micron- and submicron-thick cantilevers," *J. of Microelectromechanical Systems*, vol. 9, pp. 117–125, Mar 2000.

[22] Y. Xie, S.-S. Li, Y.-W. Lin, Z. Ren, and C.-C. Nguyen, "1.52-GHz micromechanical extensional wine-glass mode ring resonators," *IEEE Trans. on Ultrasonics, Ferroelectrics and Frequency Control*, vol. 55, pp. 890–907, April 2008.

[23] Z. Hao, Y. Xu, and S. K. Durgam, "A thermal-energy method for calculating thermoelastic damping in micromechanical resonators," *Journal of Sound and Vibration*, vol. 322, no. 4-5, pp. 870 – 882, 2009.

[24] J. Wang, Z. Ren, and C.-C. Nguyen, "1.156-GHz self-aligned vibrating micromechanical disk resonator," *IEEE Trans. on Ultrasonics, Ferroelectrics and Frequency Control*, vol. 51, pp. 1607–1628, Dec. 2004.

[25] S. Pourkamali, Z. Hao, and F. Ayazi, "VHF single crystal silicon capacitive elliptic bulk-mode disk resonators-part II: implementation and characterization," *Microelectromechanical Systems, Journal of*, vol. 13, pp. 1054–1062, Dec. 2004.

[26] W. Pang, H. Zhang, and E. S. Kim, "Micromachined acoustic wave resonator isolated from substrate," *IEEE Trans. on Ultrasonics, Ferroelectrics and Frequency Control*, vol. 52, pp. 1239–1246, Aug. 2005.

[27] O. Sahin and A. Atalar, "Simulation of higher harmonics generation in tapping-mode atomic force microscopy," *Applied Physics Letters*, vol. 79, pp. 4455–+, Dec. 2001.

[28] T. Mattila, O. Jaakkola, J. Kiihamäki, J. Karttunen, T. Lamminmäki, P. Rantakari, A. Oja, H. Seppä, H. Kattelus, and I. Tittonen, "14 MHz micromechanical oscillator," *Sensors and Actuators A: Physical*, vol. 97-98, pp. 497 – 502, 2002.

[29] S. Pourkamali, A. Hashimura, R. Abdolvand, G. Ho, A. Erbil, and F. Ayazi, "High-Q single crystal silicon HARPSS capacitive beam resonators with self-aligned sub-100-nm transduction gaps," *Microelectromechanical Systems, Journal of*, vol. 12, pp. 487–496, Aug. 2003.

[30] L.-W. Hung, C.-C. Nguyen, Y. Xie, Y.-W. Lin, S.-S. Li, and Z. Ren, "UHF Micromechanical Compound-(2,4) Mode Ring Resonators With Solid-Gap Transducers," pp. 1370–1375, 29 2007-June 1 2007.

[31] M. Demirci and C.-C. Nguyen, "Mechanically corner-coupled square microresonator array for reduced series motional resistance," *Microelectromechanical Systems, Journal of*, vol. 15, pp. 1419–1436, Dec. 2006.

[32] J. Seeger and B. Boser, "Charge control of parallel-plate, electrostatic actuators and the tip-in instability," *Microelectromechanical Systems, Journal of*, vol. 12, pp. 656–671, Oct. 2003.

[33] E. Chan and R. Dutton, "Electrostatic micromechanical actuator with extended range of travel," *Microelectromechanical Systems, Journal of*, vol. 9, pp. 321–328, Sep 2000.

[34] R. Navid, J. Clark, M. Demirci, and C.-C. Nguyen, "Third-order intermodulation distortion in capacitively-driven CC-beam micromechanical resonators," pp. 228–231, 2001.

[35] A. Alastalo, T. Mattila, and H. Seppa, "Analysis of a MEMS transmission line," *IEEE Trans. on Microwave Theory and Techniques*, vol. 51, pp. 1977–1981, Aug. 2003.

[36] D. M. Pozar, *Microwave Engineering.* John Wiley and Sons, Inc., 1998.

[37] K. F. Graff, *Wave Motion In Elastic Solids.* Clarendon Press, Oxford, 1975.

[38] V. Tas, S. Olcum, D. Aksoy, and A. Atalar, "Reducing anchor loss in micromechanical extensional mode resonators." Submitted.

[39] K. Lakin, K. McCarron, and R. Rose, "Solidly mounted resonators and filters," vol. 2, pp. 905–908 vol.2, Nov 1995.

[40] Z. Hao and Y. Xu, "Vibration displacement on substrate due to time-harmonic stress sources from a micromechanical resonator," *J. of Sound and Vibration*, vol. 322, no. 1–2, pp. 196–215, 2009.

[41] Z. Hao and F. Ayazi, "Support loss in the radial bulk-mode vibrations of center-supported micromechanical disk resonators," *Sensors and Actuators A: Physical*, vol. 134, no. 2, pp. 582–593, 2007.

[42] S. G. David S. Bindel, "Elastic PMLs for resonator anchor loss simulation," *Int. J. for Numerical Methods in Engineering*, vol. 64, pp. 789–818, 2005.

[43] R. Adler, "Compact electromechanical filters," *Electronics*, vol. 20, pp. 100–105, Apr 1947.

[44] W. P. Mason, *Electromechanical Transducers and Wave Filters.* Van Nostrand, 1942.

[45] F. Bannon, J. Clark, and C.-C. Nguyen, “High-Q HF microelectromechanical filters,” *Solid-State Circuits, IEEE Journal of*, vol. 35, pp. 512–526, Apr 2000.

[46] A. Alastalo and V. Kaajakari, “Systematic design approach for capacitively coupled microelectromechanical filters,” *Ultrasonics, Ferroelectrics and Frequency Control, IEEE Transactions on*, vol. 53, pp. 1662–1670, Sept. 2006.

[47] M. Konno, “Equivalent Electrical Network for the Transversely Vibrating Uniform Bar,” *Acoustical Society of America Journal*, vol. 38, pp. 614–+, 1965.

[48] C. T.-C. Nguyen, *Micromechanical Signal Processors.* PhD thesis, University Of California, Berkeley., 1994.

[49] S. Bhave, D. Gao, R. Maboudian, and R. Howe, “Fully-differential polysic lame mode resonator and checkerboard filter,” pp. 223–226, Jan.-3 Feb. 2005.